Advanced modeling and numerical simulations for the thermo-chemico-mechanical behaviour of materials with damage and hydrogen, based on the thermodynamics of irreversible processes

Kanssoune Saliya, Benoît Panicaud, Carl Labergere

Advanced modeling and numerical simulations for the thermo-chemico-mechanical behaviour of materials with damage and hydrogen, based on the thermodynamics of irreversible processes

K. Saliya[a], B. Panicaud[a,*], C. Labergère[a]

[a] *ICD-Lasmis, Université de Technologie de Troyes (UTT), CNRS FRE, 12 rue Marie Curie, CS 42060, 10004 Troyes, France*

Abstract

In the present article, we propose a fully coupled thermo-elasto-plastic-damage theory, which includes both kinematic and isotropic hardening, and also accounts for hydrogen diffusion in metals. This theory is based on the thermodynamics of irreversible processes under small deformation hypothesis and suppose that hydrogen diffuses in both normal interstitial lattice sites and trapping sites. This model is implemented into Abaqus/Standard by developing a UEL user subroutine and using an assumed strain method. A numerical application is performed to simulate hydrogen diffusion in a metallic welded joint submitted to a long-time severe environment at constant temperature.

Keywords: `modeling`, `diffusion`, `hydrogen embrittlement`, `mechanochemistry`, `plasticity`, `damage`, `finite elements analysis`, `ABAQUS/Implicit`

1. Introduction

One phenomenon at the origin of degradation of metals and alloys in presence of hydrogen is known as hydrogen embrittlement. Modeling the interactions between metallic materials and hydrogen is necessary in order to improve the

*Corresponding author. Tel.: +33 (0)3 25 71 80 61; fax : +33 (0)3 25 71 56 75
Email address: `benoit.panicaud@utt.fr` (B. Panicaud)

reliability and predictivity of models. So when claiming to model the mechanical behavior of metals and alloys in chemical environments, it is necessary to introduce a degree of freedom such as hydrogen concentration.

The effects of hydrogen on the physical and mechanical properties of iron and steel are quite well-known [1]. Hydrogen softens iron by enhancing screw dislocation mobility at room temperature, but hardens iron by dislocation core interactions at lower temperatures [1]. Metals and alloys are generally degraded in presence of hydrogen [1, 2, 3, 4, 5]. Embrittlement by hydrogen is explained by a great number of theories. Two of them are the most developed: hydrogen enhanced decohesion (HEDE) and hydrogen locally enhanced plasticity (HELP). On one hand, HEDE theory explains that interstitial hydrogen lowers the cohesive strength by dilatation of the atomic lattice leading to lower the fracture energy. This implies that hydrogen reduces the cohesion [6, 7]. On the other hand, HELP theory is characterized by atomic hydrogen that favors or enhances the mobility of dislocations through an elastic shielding effect in some specific crystallographic planes at the crack tip, causing locally a decrease of shear strength [5, 8, 9, 10]. To model therefore the interactions between metal and hydrogen, several authors have proposed different models for the study of hydrogen embrittlement, for example near a crack tip [5, 10, 11, 12, 13]. All these models consider two kinds of sites for hydrogen diffusion: normal interstitial lattice sites and microstructural trapping sites such as dislocation cores, grain boundaries, and interfaces between the matrix and various second-phase particles. Most of these models use the assumption of Oriani [14]: within a continuum-level material point and for a specific range of trap binding energies, the microstructure affects the local distribution of hydrogen in a manner such that the population of hydrogen in trapping sites is always in equilibrium with the population associated with normal interstitial lattice sites.

Most of the existing models, although allowing to study the effects of hydrogen diffusion on the mechanics and reciprocally, are not fully based on the thermodynamics of irreversible processes [5, 11, 13]. Only few models as the one of Di Leo [12], is based on a thermodynamically-consistent framework.

Moreover, when a material or alloy is subjected to thermomechanical loading, material/alloy may be damaged at a given moment. These damages can in turn influence the diffusion of hydrogen into the metal or alloy. It is therefore important to take also into account the damage of the material or alloy in the thermomechanical models coupled to the diffusion for a higher predictivity of the lifetime of materials.

Damage mechanics [15, 16, 17] has widely been studied and has reached now an important degree of maturity. Indeed, such a mechanical behaviour is now used for various engineering problems mainly to predict the lifetime of mechanical structures under different kinds of thermomechanical loading paths and applied to different kinds of materials such as metals, composites, ceramics, etc. (see for example [18]). The modeling of damage in metallic materials is developed following two different approaches. The first approach takes the void volume fraction as a main damage parameter governed by the initiation, growth, and coalescence of voids and their effects on the yield function and/or plastic potentials [19, 20, 21, 22, 23]. The second approach is based on the Continuum Damage Mechanics (CDM) theory assuming damage as a state variable that can be easily included in a thermodynamic framework [15, 16, 24, 25, 26, 27].

The aim of this article is to contribute to the modeling of hydrogen embrittlement in metals and alloys, by proposing a coupled mechanical-diffusion model, in which one takes into account the damage and both kinematic hardening and isotropic hardening, based on the thermodynamics of irreversible processes. The CDM theory approach is presently used for the modeling of damage.

Elasto-visco-plastic models, taking into account different hardening effects (isotropic and kinematic) in the material and strongly coupled to damage and to temperature, has been widely studied [28, 29]. Such models are frequently built on a thermodynamics framework, with temperature as external state variable to fully couple mechanics with temperature effects. Isotropic damage is often considered by the use of a CDM model, as developed by Lemaitre and Chaboche [15]. Therefore, we base our modeling development on such elasto-visco-plastic models and naturally extend it to diffusion of chemical species.

In section 2, we present the fully coupled thermo-elasto-visco-plastic damage extended to hydrogen diffusion phenomenon and the corresponding constitutive equations. In section 3, boundary conditions and numerical aspects associated to the model are deeply discussed. This mechanical-damage model coupled to hydrogen diffusion is eventually implemented in Abaqus/Standard by developing a user subroutine UEL, using an assumed strain method [30]. In section 4, we present a numerical application for hydrogen diffusion in a metallic welded joint. Conclusions and some perspectives of this work are eventually proposed.

2. Thermodynamics modeling

The theoretical framework is explained using small deformation framework, but large deformation theory is used for numerical implementation. Specifically, we consider the multiplicative decomposition of the gradient of transformation F that leads to an additive decomposition of the strain rate, the elastic strain rate being small. To ensure objectivity, we choose a corotational derivative. For numerical application, we consider the reactualized Lagrangian method. All along this article, the dot $\dot{X}$ operation corresponds to the total derivative.

The coupled model developed in the present article is a coupled thermo-mechanical-damage and diffusion model. To achieve such a goal, we base our theory on the thermodynamics of irreversible processes with state variables. The model is an extension of the fully coupled thermo-elasto-visco-plastic model including damage and both kinematic and isotropic hardening, presented in [15, 16, 28, 29], and brings some improvements to a previous work [31]. We introduce two external state variables:

- $(\underline{\varepsilon}, \underline{\sigma})$ for total strain tensor and Cauchy stress tensor;
- (T, s_e) for absolute temperature and specific entropy.

We introduce also several internal state variables:

- $(\underline{\varepsilon}^e, \underline{\sigma})$ for thermal and elastic strain tensor and Cauchy stress tensor;

- $(\vec{q}, \vec{\nabla} T)$ for heat flux vector and its conjugate thermodynamic force, the temperature gradient;

- $(\underline{\alpha}, \underline{X})$ for the back-strain and back-stress deviatoric tensors that describe the kinematic hardening;

- (r, R) for the equivalent plastic driving strain and stress that describe the isotropic hardening;

- (D, Y) for isotropic damage and its conjugate force [16]. Damage D aims at modelling a general case of damage using a phenomenological approach by use of a potential.

For diffusion, some developments of the model for several chemical species can be found in [31]. Here we focus only on hydrogen diffusion in solid materials with specific improvements. It is assumed that hydrogen has two levels of diffusion: diffusion in normal interstitial lattice sites (L) and diffusion in trapping sites (T) at microstructural defects, for example related to plastic strain. We define c_H^L the lattice hydrogen concentration, c_H^T the trapping hydrogen concentration, μ_H^L the lattice chemical potential of hydrogen and μ_H^T the trapping chemical potential of hydrogen. To describe the hydrogen diffusion phenomena in the model for both lattice and trapping sites, we introduce (c_H^L, μ_H^L) and (c_H^T, μ_H^T) as internal state variables. The multiphysic coupling of hydrogen diffusion with the damage is here performed via the thermodynamics of irreversible processes. It allows linking the effect of the damage to hydrogen diffusion, to propose a modeling of the material embrittlement by hydrogen.

2.1. Balance laws

2.1.1. Force balance

Let V be the volume of the body and ∂V his boundary. In this volume, the force balance is given by:

$$\vec{\nabla} \cdot \underline{\sigma} + \vec{f_d} = \rho \vec{\ddot{u}} \tag{1}$$

where $\vec{f}_d$ is the imposed body force vector and $\vec{u}$ is the displacement vector. The time scales associated with the diffusion of hydrogen are generally much longer than those associated with the mechanical wave propagation. So, we can neglect in the following all the effects of mechanical inertia.

2.1.2. Chemical species balance

Let $h_{L\to T}$ be the transformation rate from lattice to trapping, measured as the number of moles of solute atoms per unit of volume and per unit of time [12]. Changes in lattice hydrogen concentration c_H^L and trapping hydrogen concentration c_H^T in V are due to hydrogen diffusion across the boundary ∂V, and by $h_{L\to T}$ in V. The rates of change of lattice and trapping hydrogen in V are given through the chemical species balance, applied to hydrogen [12]:

$$\begin{cases} \dot{c}_H^L = -\vec{\nabla}\cdot\vec{J}_H^L - h_{L\to T} \\ \dot{c}_H^T = -\vec{\nabla}\cdot\vec{J}_H^T + h_{L\to T} \end{cases} \tag{2}$$

where $\vec{J}_H^L$ and $\vec{J}_H^T$ respectively represent the flux of lattice and trapping hydrogen. Theses fluxes are measured as the number of moles of solute atoms per unit of area and per unit of time. Note that the transformation rate between lattice and trapping is specifically introduced, compared to a previous work [31].

2.2. Thermodynamics laws : internal energy balance and entropy imbalance

In the absence of diffusion, the internal energy balance and the second law of thermodynamics are respectively given by Eq. 3 and Eq. 4.

$$\rho\dot{e} = \underline{\sigma} : \dot{\underline{\varepsilon}} - \vec{\nabla}\cdot\vec{q} + \pi \tag{3}$$

$$\rho\dot{s}_e \geq -\frac{1}{T}\vec{\nabla}\cdot\vec{q} + \frac{\vec{q}}{T^2}\vec{\nabla}T + \frac{\pi}{T} \tag{4}$$

where e is the specific internal energy (density per unit of mass), $\underline{\varepsilon}$ is the total strain tensor, π is the heat source in the volume V, $\vec{q}$ is the heat flux and s_e is the specific entropy. Two choices of modification a priori exist for the previous equations for accounting the presence of diffusion:

Choice 1: entropy imbalance modification. In the presence of diffusion, some authors propose to modify only the second law of thermodynamics by modifying the heat flux in Eq. 4: $\vec{q} \rightarrow \vec{q} - \mu_H^L \vec{J}_H^L - \mu_H^T \vec{J}_H^T$ [32, 33]. In this case, Eq. 4 of entropy imbalance becomes, using Eq. 2:

$$\rho \dot{s}_e \geq -\frac{1}{T}\vec{\nabla}\cdot\vec{q} + \frac{\vec{q} - \mu_H^L \vec{J}_H^L - \mu_H^T \vec{J}_H^T}{T^2}\vec{\nabla}T + \frac{\pi}{T} - \frac{1}{T}\left(\mu_H^L \dot{c}_H^L + \mu_H^T \dot{c}_H^T - \vec{\nabla}\mu_H^L.\vec{J}_H^L - \vec{\nabla}\mu_H^T.\vec{J}_H^T + (\mu_H^L - \mu_H^T)h_{L\rightarrow T}\right) \quad (5)$$

Choice 2: energy balance modification. Other authors like Di Leo [12] prefer to change only the energy balance to take into account the effects of diffusion by modifying the heat flux in Eq. 3: $\vec{q} \rightarrow \vec{q} + \mu_H^L \vec{J}_H^L + \mu_H^T \vec{J}_H^T$. It leads to the expression of the energy balance (Eq. 3) in the following form with the use of Eq. 2:

$$\rho \dot{e} = \underline{\sigma} : \underline{\dot{\varepsilon}} - \vec{\nabla}\cdot\vec{q} + \pi + \mu_H^L \dot{c}_H^L + \mu_H^T \dot{c}_H^T - \vec{\nabla}\mu_H^L.\vec{J}_H^L - \vec{\nabla}\mu_H^T.\vec{J}_H^T + (\mu_H^L - \mu_H^T)h_{L\rightarrow T} \quad (6)$$

Through additional constraints, a choice will have to be done and is further discussed.

2.3. Clausius-Duhem dissipation inequality

Dissipation inequality can be obtained here using separately the two different choices of modification (entropy imbalance modification on one hand **or** energy balance modification on the other hand).

2.3.1. With entropy imbalance modification

First we multiply Eq. 5 by T and make the difference between the obtained equation and Eq. 3. We obtain:

$$\rho(T\dot{s}_e - \dot{e}) \geq -\underline{\sigma} : \underline{\dot{\varepsilon}} + \frac{(\vec{q} - \mu_H^L \vec{J}_H^L - \mu_H^T \vec{J}_H^T)}{T}\vec{\nabla}T - \mu_H^L \dot{c}_H^L - \mu_H^T \dot{c}_H^T + \vec{\nabla}\mu_H^L.\vec{J}_H^L + \vec{\nabla}\mu_H^T.\vec{J}_H^T - (\mu_H^L - \mu_H^T)h_{L\rightarrow T} \quad (7)$$

Internal energy e is related to the thermodynamics potential ψ (Helmholtz specific free energy), the temperature T and the specific entropy s_e by the relation

$e = \psi + Ts_e$. We use the Helmholtz free energy as a state potential ψ, function of the different state variables mentioned at the beginning of this section such that: $\psi = \psi(\underline{\varepsilon}^e, \underline{\alpha}, r, D, T, c_H^L, c_H^T)$. Eq. 7 becomes:

$$\begin{aligned}(\underline{\sigma} - \rho\frac{\partial\psi}{\partial\underline{\varepsilon}^e}) : \underline{\dot{\varepsilon}}^e + \underline{\sigma} : \underline{\dot{\varepsilon}}^p - \rho(s_e + \frac{\partial\psi}{\partial T})\dot{T} - \frac{(\vec{q} - \mu_H^L\vec{J}_H^L - \mu_H^T\vec{J}_H^T)}{T}\vec{\nabla}T \\ -\rho\frac{\partial\psi}{\partial\underline{\alpha}} : \underline{\dot{\alpha}} - \rho\frac{\partial\psi}{\partial r}\dot{r} - \rho\frac{\partial\psi}{\partial D}\dot{D} + (\mu_H^L - \rho\frac{\partial\psi}{\partial c_H^L})\dot{c}_H^L + (\mu_H^T - \rho\frac{\partial\psi}{\partial c_H^T})\dot{c}_H^T \\ -\vec{\nabla}\mu_H^L.\vec{J}_H^L - \vec{\nabla}\mu_H^T.\vec{J}_H^T + (\mu_H^L - \mu_H^T)h_{L\to T} \geq 0\end{aligned} \tag{8}$$

Eq. 8 must be verified regardless of the transformation considered from the set $(\underline{\varepsilon}^e, \underline{\alpha}, r, D, T, c_H^L, c_H^T)$. In order to simplify this inequality, we take into account some classical hypotheses [34]. We can then deduce from these hypotheses, extended to diffusion, the following relations known as state relations:

$$\begin{cases} \underline{\sigma} = \rho\dfrac{\partial\psi}{\partial\underline{\varepsilon}^e} \\ s_e = -\dfrac{\partial\psi}{\partial T} \\ \underline{X} = \rho\dfrac{\partial\psi}{\partial\underline{\alpha}} \\ R = \rho\dfrac{\partial\psi}{\partial r} \\ Y = -\rho\dfrac{\partial\psi}{\partial D} \\ \mu_H^L = \rho\dfrac{\partial\psi}{\partial c_H^L} \\ \mu_H^T = \rho\dfrac{\partial\psi}{\partial c_H^T} \end{cases} \tag{9}$$

Using these state relations, the residual inequality giving the total dissipation Φ that results from the Clausius-Duhem dissipation inequality (Eq. 8) can be decomposed into the sum of mechanical Φ^m, thermal Φ^{th} and diffusion Φ^{dif} dissipations:

$$\Phi = \Phi^m + \Phi^{th} + \Phi^{dif} \geq 0 \tag{10}$$

$$with \begin{cases} \Phi^m = \underline{\sigma} : \underline{\dot{\varepsilon}}^p - \underline{X} : \dot{\alpha} - R\dot{r} + Y\dot{D} \\ \Phi^{th} = -\dfrac{\vec{q}}{T}.\vec{\nabla}T + \dfrac{1}{T}\left(\mu_H^L\vec{J}_H^L + \mu_H^T\vec{J}_H^T\right).\vec{\nabla}T \\ \Phi^{dif} = -\vec{\nabla}\mu_H^L.\vec{J}_H^L - \vec{\nabla}\mu_H^T.\vec{J}_H^T + (\mu_H^L - \mu_H^T)h_{L\to T} \end{cases} \tag{11}$$

To verify Eq. 10, a preliminary study has to be performed especially on the positivity of Eq. $(11)_b$. Therefore, with entropy imbalance modification, the residual inequality is verified only in some specific cases.

2.3.2. With energy balance modification

Following the same reasoning as previously by using Eq. 4 and Eq. 6 respectively instead of Eq. 5 and Eq. 3, we strictly find the same relations as Eq. 9, and the residual inequality resulting from the Clausius-Duhem dissipation inequality has the following form:

$$\Phi = \Phi^m + \Phi^{th} + \Phi^{dif} \geq 0 \tag{12}$$

$$with \begin{cases} \Phi^m = \underline{\sigma} : \underline{\dot{\varepsilon}}^p - \underline{X} : \dot{\alpha} - R\dot{r} + Y\dot{D} \\ \Phi^{th} = -\dfrac{\vec{q}}{T}.\vec{\nabla}T \\ \Phi^{dif} = -\vec{\nabla}\mu_H^L.\vec{J}_H^L - \vec{\nabla}\mu_H^T.\vec{J}_H^T + (\mu_H^L - \mu_H^T)h_{L\to T} \end{cases} \tag{13}$$

Unlike the case with entropy imbalance modification, with energy balance modification the residual inequality is now verified for all cases of transformation.

Whether considering the entropy imbalance modification [32, 33] or the energy balance modification [12], both lead almost to the same result in the Clausius-Duhem inequality. The only difference comes in the expression of thermal dissipation Φ^{th}. Especially, it will lead strictly to the same expressions for isothermal transformations. If needed, choice 2 (energy balance modification) will be systematically chosen.

The different dissipations have now to be separately analyzed in order to derive the flux variables $\left(\underline{\dot{\varepsilon}}^p, \underline{\dot{\alpha}}, \dot{r}, \dot{D}, \frac{\vec{q}}{T}, \dot{c}_H^L, \dot{c}_H^T\right)$.

2.4. Expression of state relations

2.4.1. State potential specification

The state potential is taken as Helmholtz specific free energy ψ as a function of the different state variables, $\psi = \psi(\underline{\varepsilon}^e, \underline{\alpha}, r, D, T, c_H^L, c_H^T)$. In the present isotropic case, we consider the free energy as a sum of three energies: thermoelastic (e), plastic (p) and diffusion energies (dif). For convenience, we use

exponent e for energy or strain, but we have to keep in mind that it corresponds to thermal and elastic energy or strain.

$$\rho\psi = \rho\psi^e + \rho\psi^p + \rho\psi^{dif} \tag{14}$$

Considering scalar arguments to be used with the representation theorem [35], we define:

$$\rho\psi^e = \begin{cases} \dfrac{1-D}{2}\left(\lambda(\underline{\varepsilon}^e : \underline{1})^2 + 2\mu\underline{\varepsilon}^e : \underline{\varepsilon}^e\right) - 3K\vartheta\Delta T\sqrt{1-D}\underline{\varepsilon}^e : \underline{1} \\ -\rho C_v T\left[\ln\left(\dfrac{T}{T_0}\right) - 1\right] - 3K\beta(\Delta c_H^L + \Delta c_H^T)\sqrt{1-D}\underline{\varepsilon}^e : \underline{1} \end{cases} \tag{15}$$

with $\Delta T = T - T_0$, $\Delta c_H^L = c_H^L - c_{H0}^L$ and $\Delta c_H^T = c_H^T - c_{H0}^T$. T_0 is the reference temperature, c_{H0}^L and c_{H0}^T are respectively the initial lattice and trapping hydrogen concentration.

$$\rho\psi^p = \frac{1}{3}C(1-D)\underline{\alpha} : \underline{\alpha} + \frac{1}{2}(1-D^\gamma)Qr^2 \tag{16}$$

where γ is a material feature, which allows to slow down the contribution of the isotropic hardening in the driving energy of damage. Note also that this parameter has not been introduced in a previous work [31] and constitutes a specificity of the present modelling.

$$\rho\psi^{dif} = \begin{cases} \mu_{H0}^L c_H^L + R_g T\left[c_H^L \ln\left(\dfrac{c_H^L}{N^L}\right) + (N^L - c_H^L)\ln\left(1 - \dfrac{c_H^L}{N^L}\right)\right] \\ +\mu_{H0}^T c_H^T + R_g T\left[c_H^T \ln\left(\dfrac{c_H^T}{N^T}\right) + (N^T - c_H^T)\ln\left(1 - \dfrac{c_H^T}{N^T}\right)\right] \end{cases} \tag{17}$$

In the previous equations, ρ is the material density, λ and μ are the Lamé 's constants for linear, homogeneous and isotropic elasticity, K is the bulk modulus ($K = ((3\lambda + 2\mu))/3$), C_v is the specific heat coefficient, Q and C are respectively the isotropic and kinematic hardening moduli. ϑ and β are respectively the thermal and the chemical expansion coefficients, and R_g is the universal constant of perfect gases ($R_g = 8.314\,462\,1\,\mathrm{J\,mol^{-1}K^{-1}}$). As noted in [12], for the chemical expansion coefficient, there is insufficient information from either experiments or micromechanical models concerning the nature and amount of chemical expansion caused by the trapped hydrogen. So, for simplicity in Eq.

15, we suppose that the amount of chemical expansion caused by the trapped hydrogen is the same as the one caused by the lattice hydrogen. N^L is the number of moles of lattice sites per unit reference volume. This is a property of the host metal and calculated by $N^L = N_A/V_M$, with N_A the Avogadro 's number and V_M the molar volume of the host lattice. N^L is therefore constant. N^T is the number of moles of trapping sites per unit of reference volume, whose experiments show that it is a function of plastic strain. Let θ_H^L and θ_H^T denote respectively the occupancy fraction of the lattice and trapping sites ($0 \leq \theta_H^L \leq 1$ and $0 \leq \theta_H^T \leq 1$). They are directly related to its corresponding concentration by: $c_H^L = \theta_H^L N^L$ and $c_H^T = \theta_H^T N^T$.

Note that in Eq. 15, damage is introduced through the thermo-elastic strain. Moreover, we suppose that damage has no direct influence on the thermal and chemical state variables. This aspect will be investigated in a further article. The free energy that we define can be therefore interpreted as a generalization of the thermo-elasto-visco-plastic energy function of the isotropic damage [28], extended to the diffusion.

2.4.2. State relations

By introducing the above state potential into the modified Clausius-Duhem inequality, the following state relations are obtained by considering the Clausius-Duhem relation in the case of irreversible transformations (i.e. without dissipation).

- Cauchy stress tensor

$$\begin{aligned} \underline{\sigma} = \rho \frac{\partial \psi}{\partial \underline{\varepsilon}^e} &= (1-D)\left(\lambda(\underline{\varepsilon}^e : \underline{1})\underline{1} + 2\mu\underline{\varepsilon}^e\right) \\ &\quad -3K\sqrt{1-D}\left(\vartheta\Delta T + \beta(\Delta c_H^L + \Delta c_H^T)\right)\underline{1} \end{aligned} \tag{18}$$

- Specific entropy

$$\begin{aligned} s_e = -\frac{\partial \psi}{\partial T} &= \frac{3}{\rho} K \vartheta \sqrt{1-D}\underline{\varepsilon}^e : \underline{1} + C_v \ln\left(\frac{T}{T_0}\right) \\ &\quad -\frac{R_g}{\rho}\left[c_H^L \ln\left(\frac{c_H^L}{N^L}\right) + (N^L + c_H^L)\ln\left(1-\frac{c_H^L}{N^L}\right)\right] \\ &\quad -\frac{R_g}{\rho}\left[c_H^T \ln\left(\frac{c_H^T}{N^T}\right) + (N^T + c_H^T)\ln\left(1-\frac{c_H^T}{N^T}\right)\right] \end{aligned} \tag{19}$$

- Kinematic or back stress tensor

$$\underline{X} = \rho\frac{\partial \psi}{\partial \underline{\alpha}} = \frac{2}{3}C(1-D)\underline{\alpha} \tag{20}$$

- Isotropic stress

$$R = \rho\frac{\partial \psi}{\partial r} = Q(1-D^\gamma)r \tag{21}$$

- Damage conjugate force

$$Y = -\rho\frac{\partial \psi}{\partial D} = Y_e + Y_p + Y_d \tag{22}$$

with ($\theta_H^T = \frac{c_H^T}{N^T}$):

$$\begin{cases} Y_e = \dfrac{1}{2}\lambda(\underline{\varepsilon}^e : \underline{1})^2 + \mu\underline{\varepsilon}^e : \underline{\varepsilon}^e - \dfrac{3K\vartheta\Delta T}{2\sqrt{1-D}}\underline{\varepsilon}^e : \underline{1} \\ -\dfrac{3K\beta(\Delta c_H^L + \Delta c_H^T)}{2\sqrt{1-D}}\underline{\varepsilon}^e : \underline{1} + 3K\beta\dfrac{\partial \Delta c_H^T}{\partial D}\sqrt{1-D}\underline{\varepsilon}^e : \underline{1} \\ Y_p = \dfrac{1}{3}C\underline{\alpha} : \underline{\alpha} + \dfrac{1}{2}\gamma D^{\gamma-1}Qr^2 \\ Y_d = -\dfrac{\partial}{\partial D}\left(\mu_{H0}^T c_H^T + R_g T N^T\left[\theta_H^T \ln\left(\theta_H^T\right) + (1-\theta_H^T)\ln\left(1-\theta_H^T\right)\right]\right) \end{cases} \tag{23}$$

- Lattice chemical potential

$$\mu_H^L = \rho\frac{\partial \psi}{\partial c_H^L} = \mu_{H0}^L + R_g T \ln\left(\frac{\theta_H^L}{1-\theta_H^L}\right) - 3K\beta\sqrt{1-D}\underline{\varepsilon}^e : \underline{1} \tag{24}$$

- Trapping chemical potential

$$\mu_H^T = \rho\frac{\partial \psi}{\partial c_H^T} = \mu_{H0}^T + R_g T \ln\left(\frac{\theta_H^T}{1-\theta_H^T}\right) - 3K\beta\sqrt{1-D}\underline{\varepsilon}^e : \underline{1} \tag{25}$$

Contrarily to other works, which are not based on the thermodynamics of irreversible processes with coupling between mechanics and diffusion

[5, 13], the influence of the mechanical state on the hydrogen diffusion here is explicitly related to the thermo-elastic strain tensor and not to Cauchy stress tensor through chemical potentials expressions (Eqs. 24 and 25).

2.5. Mechanical dissipation and hydrogen induced softening

2.5.1. Mechanical equations for dissipation

For the mechanical dissipation, the derived equations from our model are those already described by many authors [16, 26, 27, 28]. Furthermore, it is also required for calculations to give the definition of the yield function and the damage evolution. The yield function associated to our model is described through the von Mises criterion:

$$f = \frac{J_2(\underline{\sigma} - \underline{X})}{\sqrt{1-D}} - \frac{R}{\sqrt{1-D^{\gamma}}} - \sigma_Y \leq 0 \tag{26}$$

where σ_Y is the yield strength and J_2 is the second invariant of the stress tensor or equivalent stress of von Mises, defined for any second-rank stress-like tensor $\underline{M}$ by:

$$J_2(\underline{M}) = \sqrt{\frac{2}{3}(\underline{M})^{dev} : (\underline{M})^{dev}} \tag{27}$$

dev in exponent denotes the deviatoric part of the tensor. The damage evolution model is obtained using the generalized normality [16, 26, 28]:

$$\dot{D} = \frac{\dot{\delta}}{(1-D)^{\beta}} \left[\frac{\langle Y - Y_0 \rangle}{S} \right]^{s} \tag{28}$$

S, s, Y_0 and β in Eq. 28 are material coefficients characterizing the damage evolution and $\dot{\delta}$ is the Lagrange multiplier [16, 26]. For more information on the mechanical equations for dissipation, the reader can refer to the specific references [16, 26, 27, 28, 36, 37].

2.5.2. Hydrogen induced softening

In the present article, yield strength is modified by environment effects. Indeed, experimentally, Birnbaum and Sofronis [8] demonstrated that hydrogen

enhances dislocation motion causing a local softening. To model this effect of hydrogen, Sofronis [5] expresses the local flow stress as a function of the total concentration of hydrogen $C_H = (c_H^L + c_H^T)/N^L$ in metal and the equivalent plastic strain ε^p:

$$\sigma_Y(\varepsilon^p, C_H) = [(\xi - 1)C_H + 1]\,\sigma_0 \left(1 + \frac{\varepsilon^p}{\varepsilon_0}\right)^{1/m} \tag{29}$$

with σ_0 the initial yield strength in absence of hydrogen, ε_0 the initial yield strain in absence of hydrogen, m the hardening exponent. The parameter ξ is supposed to be positive and less than unity.

In the present model, the same effects of hydrogen on the metal are considered. But in view of the elasto-plastic model that we use here, we express the yield strength σ_Y in the following form:

$$\sigma_Y(C_H) = [(\xi - 1)C_H + 1]\,\sigma_{Y_0} \tag{30}$$

with σ_{Y_0} the initial yield strength in absence of hydrogen. The plastic effect in Eq. 29 already being taken into account in the yield function (Eq. 26) with the isotropic stress R calculated from Eq. 21. Note that apart the Eq. 30 modeling hydrogen induced softening, another phenomenon due to hydrogen is taken into account: hydrogen induced dilation, given by Eq. 18 of Cauchy stress tensor. Eqs. 22 and $(23)_c$ also show a possible influence of hydrogen on the damage evolution.

2.6. Thermal equations for dissipation

It requires first to express the heat equation. To establish thermal heat equation, on one hand, we express entropy s_e as a function of the different state variables. On the other hand, we use Eq. 3 if one uses the entropy imbalance modification or Eq. 6 if one uses energy balance modification. The last one has been chosen because of its more general capability to validate residual dissipation inequality.

With energy balance modification. In the case of energy balance modification, the internal energy equation in the presence of the diffusion of species is modified. So using Eq. 6 and replacing $\dot{e}$ by $\dot{\psi} + \dot{T}s_e + T\dot{s}_e$ and $\dot{\psi}$ by its expression as a function of the different state variables, we obtain (using Eq. 9) the generalized heat equation in a thermo-elasto-inelastic-damage solid coupled with diffusion in this form:

$$\rho C_v \dot{T} = -\vec{\nabla} \cdot \vec{q} + R_{pl} + \pi \tag{31}$$

where R_{pl} is now given by:

$$R_{pl} = \Phi^m + T\left(\frac{\partial \underline{\sigma}}{\partial T} : \underline{\dot{\varepsilon}}^e + \frac{\partial \underline{X}}{\partial T} : \underline{\dot{\alpha}} + \frac{\partial R}{\partial T}\dot{r} - \frac{\partial Y}{\partial T}\dot{D} + \frac{\partial \mu_H^L}{\partial T}\dot{c}_H^L + \frac{\partial \mu_H^T}{\partial T}\dot{c}_H^T\right) - \vec{\nabla}\mu_H^L.\vec{J}_H^L - \vec{\nabla}\mu_H^T.\vec{J}_H^T + (\mu_H^L - \mu_H^T)h_{L\to T} \tag{32}$$

Φ^m in Eq. 31 is the mechanical dissipation defined in Eq. 11 or Eq. 13.

In order to take correctly into account all the multi-physical effects, the heat flux vector $\vec{q}$ must now also depends not only on the gradient of temperature, but also on the chemical potential gradient of each species by application of the thermodynamics of irreversible processes (Onsager's principle as detailed in [38, 33, 32]), without coupling with pressure :

$$\vec{q} = -L_{TH}^L \vec{\nabla}\mu_H^L - L_{TH}^T \vec{\nabla}\mu_H^T - L_{TT}\vec{\nabla}T \tag{33}$$

with L_{TH}^L, L_{TH}^T, L_{TT} the so called kinetic coefficients of Onsager. Eq. 31 can therefore be used to derive the weak variational functional associated with the thermal problem.

2.7. Diffusion equations for dissipation

In this subsection, we analyze hydrogen diffusion in order to see the evolution of its different concentrations (lattice and trapping sites concentration) in the material with time.

The phenomenological model of volume diffusion is described in the present model not only as a function of the gradient of the chemical potentials, but also as a function of temperature (thermodiffusion) and pressure (barodiffusion)

gradients. In the literature, the influence of these last gradients is often ignored because the simulations are of too short duration (in days). For the applications of our model, simulation time can exceed the usual durations (in years). In this case, it is then assumed that barodiffusion and thermodiffusion may have a significant influence. In the general, the mechanism of diffusion in trapping sites are often negligible. In the present article, for reasons of numerical tests, we suppose that hydrogen can also diffuse inside trapped sites. From a modelling point of view, it can be relevant when describing important spatial extended defects that can trap hydrogen. For hydrogen, we define therefore the fluxes in lattice and trapping sites respectively by Eq. 34 and Eq. 35 [38].

$$\vec{J}_H^L = -L_H^L \vec{\nabla}\mu_H^L - L_{Hp}^L \vec{\nabla}p - L_{HT}^L \vec{\nabla}T \tag{34}$$

$$\vec{J}_H^T = -L_H^T \vec{\nabla}\mu_H^T - L_{Hp}^T \vec{\nabla}p - L_{HT}^T \vec{\nabla}T \tag{35}$$

where L_H^L, L_H^T, L_{Hp}^L, L_{Hp}^T, L_{HT}^L, L_{HT}^T are the kinetic coefficients of Onsager. Chemical potentials expressions are given by Eq. 24 and Eq. 25. These expressions of fluxes assume that the gradient of interstitial chemical potential does not affect flux in trapping sites and reciprocally.

Using Eq. 24 and Eq. 25 in Eq. 34 and Eq. 35, and basing the calculations on the formulation and hypotheses of Philibert [38], the diffusion coefficients (for lattice sites and for trapping sites) are expressed as functions of temperature and concentrations [31] (for $\theta_H^L < 1$ and $\theta_H^L < 1$):

$$\begin{cases} D_H^L = \dfrac{D_{H0}^L}{\Omega_H c_H^L (1-\theta_H^L)} \exp(-\dfrac{\Delta G}{R_g T}) \\ D_H^T = \dfrac{D_{H0}^T}{\Omega_H c_H^T (1-\theta_H^T)} \exp(-\dfrac{\Delta G}{R_g T}) \end{cases} \tag{36}$$

Ω_H is the partial molar of hydrogen and ΔG the variation of the free energy of Gibbs.

The local balance equation for hydrogen can be written in a single equation as the sum of the two mass balances (mass balance in lattice and in trapping sites given in Eq. 2):

$$\dot{c}_H^L + \dot{c}_H^T + \vec{\nabla} \cdot \vec{J}_H^L + \vec{\nabla} \cdot \vec{J}_H^T = 0 \tag{37}$$

Based on the classical and widely-used Orianis postulate of "local equilibrium" between lattice and trapping ($\mu_H^L = \mu_H^T$) [14], we model the concentration of trapping, supposing $\theta_H^L \ll 1$ by [39, 40]:

$$c_H^T = \frac{N^T c_H^L K^T}{c_H^L K^T + N^L} \tag{38}$$

where $K^T = \exp(\frac{\Delta\mu_H^b}{R_g T})$ and $\Delta\mu_H^b = \mu_{H0}^L - \mu_{H0}^T$ is the trapping binding energy of hydrogen. The number of moles of lattice sites N^L is supposed to be constant. According to previous works [40], the number of moles of trapping sites depends on plastic strain ($N^T = N^T(\varepsilon^p)$) and can be modeled by:

$$N^T = exp\left(23.26 - 2.33exp(-5.5\varepsilon^p)\right) log(10) \tag{39}$$

N^T in Eq. 39 is in $trap/m^3$. In the presence of damage, as proposed in this article, plastic strain is modified, therefore N^T will also depend on damage via plastic strain. The presence of damage will increase the number of moles of trapping sites (damage might acts as new traps). With this definition of N^T, and using Eq. 38, the evolution of c_H^T is then given by:

$$\dot{c}_H^T = \frac{\partial c_H^T}{\partial c_H^L}\dot{c}_H^L + \frac{\partial c_H^T}{\partial N^T}\frac{dN^T}{d\varepsilon^p}\dot{\varepsilon^p} + \frac{\partial c_H^T}{\partial K^T}\frac{dK^T}{dT}\dot{T} \tag{40}$$

Replacing Eq. 40 in Eq. 37 and after some calculations, we obtain the evolution of c_H^L as:

$$D^*\dot{c}_H^L + \theta_H^T\frac{dN^T}{d\varepsilon^p}\dot{\varepsilon^p} - \frac{c_H^T(1-\theta_H^T)\Delta\mu_H^b}{RT^2}\dot{T} + \vec{\nabla}\cdot\vec{J_H^L} + \vec{\nabla}\cdot\vec{J_H^T} = 0 \tag{41}$$

with $D^* = 1 + \frac{c_H^T(1-\theta_H^T)}{c_H^L}$.

Eq. 38 and Eq. 41 will be used to analyze hydrogen diffusion in material.

3. Boundary conditions and numerical aspects

In our application in this article, only the mechanical-diffusion model is tested. So, in the following sections we describe the fully coupled thermo-mechanical-diffusion model presented above at constant temperature.

3.1. Boundary conditions

We need now to write initial and boundary conditions to complete the modeling described above. We add therefore the usual boundary conditions (Dirichlet and Neumann) to complete the theory. Let V be the volume of the body and $S = \partial V$ be the boundary of the body.

Mechanical boundary conditions. Let S_u, S_F and S_c be the parts of boundary S where the displacement $\vec{u}$, the traction forces $\vec{t}$ and the contact forces $\vec{t_c}$ are prescribed respectively: $\vec{u} = \vec{u}_s$ on S_u, $\underline{\sigma} \cdot \vec{n} = \vec{t}$ on S_F and $\underline{\sigma} \cdot \vec{n} = \vec{t_c}$ on S_c; with $S = S_u \bigcup S_F \bigcup S_c$ and $S_u \bigcap S_F \bigcap S_c = \emptyset$.

Diffusion boundary conditions. Let S_{cL} be the part of the boundary S where hydrogen lattice concentration is imposed and S_{J_L} be the part of the boundary S where hydrogen diffusion flux in lattice sites is prescribed: $c_H^L = c_H^{Le}$ on S_{cL} and $\vec{J}_H^L \cdot \vec{n} = \vec{J}_H$ on S_{J_L}; with $S_{cL} \bigcup S_{J_L} = S$ and $S_{cL} \bigcap S_{J_L} = \emptyset$. Lattice concentration is the only quantity to solve, therefore we do not need boundary conditions for trapping sites. Considering the equilibrium between the dissolved hydrogen and its gas H_2, which leads to an equality between the different chemical potentials ($\mu_H^L = \mu_{H_2}$), we obtain the c_H^{Le} value to be applied for Dirichlet boundary conditions. For more information, see details in [12, 13].

3.2. Numerical aspects

3.2.1. Variational formulation

The associated initial and boundary value problem is decomposed into two coupled variational problems: the mechanical problem defined by the principle of virtual power based on Eq. 1 and the diffusion problem based on the local balance equation for the hydrogen lattice concentration (Eq.40). Let δu and δc_H^L be respectively the virtual displacement field and the virtual lattice hydrogen concentration, verifying the previous boundary conditions. The two variational problems are given, using the boundary conditions defined in 3.1 and by applying

the divergence theorem, by:

$$F(\vec{u}, c_H^L, \delta\vec{u}) = \int_V \underline{\sigma} : \delta\underline{D}^e dV - \int_V \vec{f}_d.\delta\vec{u}dV$$
$$- \int_{S_F} \vec{t}.\delta\vec{u}dS - \int_{S_c} \vec{t}_c.\delta\vec{u}dS + \int_V \rho\ddot{\vec{u}}.\delta\vec{u}dV \quad (42)$$

and

$$H(\vec{u}, c_H^L, \delta c_H^L) = \int_V (\delta c_H^L)^T D^* \dot{c}_H^L dV + \int_V (\delta c_H^L)^T \theta_H^T \frac{dN^T}{d\varepsilon^p}\frac{d\varepsilon^p}{dt}dV$$
$$- \int_V \vec{\nabla}(\delta c_H^L)^T (\vec{J}_H^L + \vec{J}_H^T)dV + \int_{S_{JL}} (\delta c_H^L)^T \vec{J}_H dS \quad (43)$$

where $\delta\underline{D}^e$ and $\delta\vec{u}$ are respectively the virtual strain rates and the velocity field of virtual displacements.

3.2.2. Global resolution strategy

We use here the same interpolation functions N_i to approximate both the displacement and the diffusion fields inside each isoparametric finite elements (FE). We neglect all the effects of inertia ($\ddot{\vec{u}} = \vec{0}$) without imposed force ($\vec{f}_d = \vec{0}$) and with $\vec{t} = \vec{t}_c = \vec{0}$, no hydrogen flow is imposed ($\vec{J}_H = \vec{0}$). By using the displacement-based FE method, two functionals have to be defined, for each element (e) in its current (deformed, damaged, and corroded) configuration with volume V and boundary S:

$$\{R_M\} = \int_V [B_M]^T \{\sigma\} dV \quad (44)$$

and

$$\{R_D\} = \int_V \{N\} D^* \langle N \rangle dV \{\dot{c}_H^L\} + \int_V \{N\} \theta_H^T \frac{dN^T}{d\varepsilon^p}\frac{d\varepsilon^p}{dt}dV$$
$$- \int_V [B_D]^T \{J_H^L + J_H^T\} dV \quad (45)$$

The standard matrix notations are used in the previous equations (Eqs. 44 and 45). The matrix $[B_M]$ is the matrix of interpolation for the total strain tensor. This matrix corresponds to the matrix $[\bar{B}]$ of equation 34 in the work of Wang [30]. The author has proposed a quadrature assumed strain mixed

element formulation to avoid hourglass modes and volumetric locking as well as shear locking. The matrix $[B_D]$ is the matrix of interpolation concerning the derivatives of diffusion fields. By using the classical assembly procedure, for the static implicit resolution, a highly nonlinear algebraic system is obtained from Eqs. 44 and 45 in this form:

$$\begin{bmatrix} K_{MM} & 0 \\ 0 & K_{DD} \end{bmatrix} \begin{Bmatrix} \Delta u \\ \Delta c_H^L \end{Bmatrix} = - \begin{Bmatrix} R_M \\ R_D \end{Bmatrix} \tag{46}$$

where K_{MM} is the tangent sub-matrix relative to the purely mechanical problem and calculated from R_M:

$$K_{MM} = \left[\frac{\partial R_M}{\partial u} \right] = \int_V [B_M]^T \frac{\partial \{\sigma\}}{\partial \{\varepsilon\}} [B_M] dV \tag{47}$$

K_{DD} is the tangent sub-matrix relative to the purely diffusion problem and calculated from R^D:

$$K_{DD} = \left[\frac{\partial R_D}{\partial c_H^L} \right] = \int_V \{N\} \frac{D^*}{\Delta t} \langle N \rangle dV + \int_V \{N\} \frac{\partial D^*}{\partial c_H^L} \frac{\Delta c_H^L}{\Delta t} \langle N \rangle dV$$
$$+ \int_V \{N\} \theta_H^T \frac{\partial}{\partial c_H^L} \left(\frac{dN^T}{d\varepsilon^p} \frac{d\varepsilon^p}{dt} \right) \langle N \rangle dV - \int_V [B]^T \frac{\partial \{J_H^L + J_H^T\}}{\partial c_H^L} \langle N \rangle dV \tag{48}$$

The tangent sub-matrices of the mechanical-diffusion coupling are neglected to allow having fewer iterations number (7 iterations on average) and then spare time calculation. Indeed, a calculation test has been initially performed without neglecting sub-matrices of the mechanical-diffusion coupling (more than 10 iterations) and has showed no influence on the results.

According to the static implicit resolution method, the system provided by Eq. 46 is solved successively over each time step. It should be noted that the variation in concentration will be much smaller than the variation in displacement. Thus the numerical resolution requires to normalize concentration by a coefficient that will be multiplied to the diffusion residue $\{R_D\}$ and to the tangent sub-matrix relative to the purely diffusion problem $[K_{DD}]$, for a better resolution of the system.

Concerning the local integration of the fully coupled constitutive equations, we extend the methodology described in [28, 41] to diffusion aspects. Elastic prediction and plastic correction description can be read in this later references.

3.3. Implementation strategy in Abaqus/standard FEM software

3.3.1. Numerical computation of the strain rate tensor

For metal part, it is crucial to consider the context of finite transformations for any behavior model that uses tensorial state variables. Accordingly, the formulation of nonlinear constitutive equations for inelastic solids under finite transformations faces two basic problems:

- How could we decompose the total strain tensor into reversible and irreversible part?
- Which formalism should we use in order to formulate the constitutive equations fulfilling the objectivity requirement?

These two aspects are widely discussed in the literature and an analysis can be found in [29, 42, 43].

In this work we consider the framework of elastoplastic finite strains based on the classical multiplicative decomposition of the total transformation gradient $\underline{F}$ into elastic $\underline{F}^e$ and plastic $\underline{F}^p$ parts [44], i.e. $\underline{F} = \underline{F}^e \underline{F}^p$.

Despite the fact that the choice of a purely Eulerian formalism leads to the best description of the finite transformations on the current deformed configuration, crucial problems of objectivity could appear. Objectivity problems posed by a reactualized Lagrangian formalism, which consists of working on the initial configuration, lead to very complex constitutive equations. In order to fulfill the objectivity requirement, the concept of the rotated frame formulation is used. This supposes that all the constitutive equations will be written on the current configuration locally rotated by the orthogonal rotation tensor $\underline{Q}$ [29, 42, 45, 46, 47], where the rotated configuration is Lagrangian by its orientation and Eulerian by the eigenvalues of the physical quantities. This rotation could be defined by two different ways. The first consists of using a privileged frame and calculating its rotation while it moves. This privileged frame is generally defined by the material microstructure as the crystallographic orientation

for the monocrystalline materials. The second relies on postulating, a priori, a kinematic equation that governs the evolution of the orthogonal tensor $\underline{Q}$:

$$\underline{\dot{Q}Q}^T = \underline{W}_Q \qquad \underline{Q}(t_0) = \underline{1} \tag{49}$$

where W_Q characterizes the choice of the rotated frame. For any second-rank tensor $\underline{T}$ defined in the current configuration, its transfer to the locally rotated configuration ($\bar{C}_t$ or $\bar{C}_t^p$) by the rotation tensor $\underline{Q}$ according to:

$$\underline{\bar{T}} = \underline{Q}^T \underline{T} \underline{Q} \tag{50}$$

$$\underline{\bar{D}} = \underline{\dot{\bar{\varepsilon}}}^e + 2\left[\underline{\bar{D}}^e \underline{\bar{W}}^p\right]^s = \underline{\dot{\bar{\varepsilon}}}^{eJ_T} + \underline{\bar{D}}^p \tag{51}$$

with $\underline{\dot{\bar{\varepsilon}}}^{eJ_T}$ being the Jaumann derivative with respect to $\underline{\bar{W}}$.

To integrate the behavior model, in the case of large deformations and rotations, it is important to choose a kinematic approximation over a time step to evaluate the strain rate tensor $\underline{D}_{n+1/2}$, according to an incrementally objective integration algorithm. The most usual approach is to proceed by the calculation of the material position and to sequence as follows:

$$\vec{x}_{n+1} = \vec{x}_n + \Delta\vec{u}_{n+1} \tag{52}$$

The transformation tensor at the time t_{n+1} is written in the following form:

$$\underline{F}_{n+1} = \frac{\partial \vec{x}_{n+1}}{\partial \vec{X}} = \frac{\partial \vec{x}_{n+1}}{\partial \vec{x}_n}\frac{\partial \vec{x}_n}{\partial \vec{X}} = \Delta\underline{F}_{n+1}\underline{F}_n = \left(\underline{I} + \frac{\partial \vec{u}_{n+1}}{\partial \vec{x}_n}\right)\underline{F}_n \tag{53}$$

Nevertheless, assuming the hypothesis of approximation of the real path by a linear scheme at constant velocity, the scheme under consideration causes a variation of volume. Hughes and Winget [48] then propose as linear relation the following expression:

$$\vec{x}_{n+\theta} = \vec{x}_n + \theta\Delta\vec{u}_{n+1} \tag{54}$$

$$\underline{F}_{n+\theta} = \Delta\underline{F}_{n+\theta}\underline{F}_n = \frac{\partial \vec{x}_{n+\theta}}{\partial \vec{x}_n}\underline{F}_n \tag{55}$$

We use a half-step implementation scheme assuming an implicit Euler scheme in time with $\theta = \frac{1}{2}$.

The gradient tensor of strain velocities can be decomposed in part symmetric and antisymmetric. The symmetrical part of the tensor is the total deformation rate, noted as $\underline{D}_{n+1/2}$, described as:

$$\underline{D}_{n+1/2} = \frac{1}{2}\left(\underline{L}_{n+1/2} + \underline{L}^T_{n+1/2}\right) \tag{56}$$

In the same way, we express the rate of rotation, noted $\underline{\omega}_{n+1/2}$, by:

$$\underline{\omega}_{n+1/2} = \frac{1}{2}\left(\underline{L}_{n+1/2} - \underline{L}^T_{n+1/2}\right) \tag{57}$$

3.3.2. A 4-node quadrilateral assumed strain element

We propose the numerical development of a multiphysic quadrilateral 2D mechanical/diffusion element. The mechanical part of this element is inspired from the work of Wang [30] and we have added the diffusion part and the mechanical/diffusion coupling contribution.

Mechanical aspects of the numerical derivation. An "assumed strain" formulation has been selected to build the mechanical part of the element to avoid the occurrence of volumetric expansion locking and shear locking. A modified Hu-Washizu's variational principle initially proposed by Fish and Belytschko [49] is used in the case of quasi-static simplification. We start from there in order to derive the following form on an elementary volume:

$$\int_{\Omega^e} \underline{\sigma}^a : \delta\underline{\dot{\varepsilon}}^a d\Omega + \delta \int_{\Omega^e} \underline{\sigma}^a : (\underline{\nabla}^s(\vec{\dot{u}}) - \underline{\dot{\varepsilon}}^a) d\Omega - \delta W_{ext} = 0 \tag{58}$$

where, δ denotes a variation, $\underline{\dot{\varepsilon}}^a$ is the assumed strain rate tensor, $\underline{\sigma}^a$ the assumed stress tensor evaluated by the constitutive model and $\underline{\nabla}^s(\vec{\dot{u}})$ the symmetric part of the velocity gradient.

We discretize this variational form in an elementary domain Ω^e and we focus on a typical element (e) between the instants t_n and t_{n+1} by switching to matrix notations ($\{V\}$ for column vector and $\langle V\rangle$ for line vector). Simo and Hughes [50] suggested the projection of the discretized velocity gradient $[B_{n+1/2}]$, so that $\{\underline{\nabla}^s(\vec{\dot{u}}^e)\}_{n+1} = [B_{n+1/2}]\{\dot{u}^e\}_{n+1/2}$. This new operator $[B^a_{n+1/2}]$ is chosen to evaluate the assumed strains rate tensor $\{\dot{\varepsilon}^a\}_{n+1} = [B^a_{n+1/2}]\{\dot{u}^e\}_{n+1/2}$ as

well as to generate an assumed stress tensor $\{\sigma^a_{n+1}\}$ orthogonal to the difference between the symmetric part of the velocity gradient and the assumed strain rate tensor. This choice allows us to simplify the Hu-Washizu variational principle and rewrite it under the following form:

$$\int_{\Omega^e} \underline{\sigma}^a : \delta\dot{\underline{\varepsilon}}^a d\Omega = \delta W_{ext} \tag{59}$$

By considering the four-node quadrilateral element given in Fig. 1, the isoparametric shape functions of the element for the displacement field in the reference space are expressed as:

$$N_i(\xi,\eta) = \frac{1}{4}(1+\xi_i\xi)(1+\eta_i\eta) \tag{60}$$

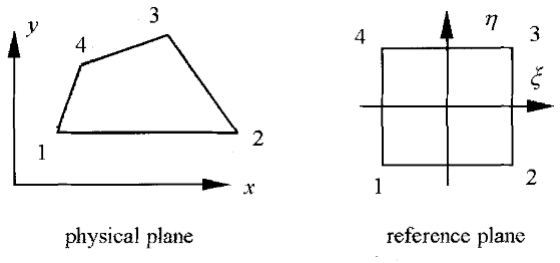

Figure 1: The quadrilateral element.

All the above shape functions can also be expanded in terms of a set of orthogonal base vectors as:

$$\{N(\xi,\eta)\} = \frac{1}{4}\{s\} + \frac{1}{4}\{\xi\}\xi + \frac{1}{4}\{\eta\}\eta + \frac{1}{4}\{h\}\xi\eta \tag{61}$$

where $\langle\xi\rangle = \langle\ -1 \quad 1 \quad 1 \quad -1\ \rangle$ and $\langle\eta\rangle = \langle\ -1 \quad -1 \quad 1 \quad 1\ \rangle$ are the vectors of the nodal co-ordinates in the reference space and, $\langle s\rangle = \langle\ 1 \quad 1 \quad 1 \quad 1\ \rangle$ and $\langle h\rangle = \langle\ 1 \quad -1 \quad 1 \quad -1\ \rangle$ are the translation and the hourglass vectors respectively.

To ensure the objectivity conditions of the model, we use a corotational system defined in the centroid of the element (see Fig. 2) built by the shape functions defined in the reference space (ξ,η). The orientation of this corotational triad is governed by the orthogonal rotation tensor $\underline{Q}$, which is expressed

under the following form:

$$[Q] = \begin{bmatrix} e_1^1 & e_1^2 \\ e_2^1 & e_2^2 \end{bmatrix}, \vec{g}_1 = \frac{\partial x}{\partial \xi}\vec{x} + \frac{\partial x}{\partial \eta}\vec{y}, \vec{e}_1 = \frac{\vec{g}_1}{\|\vec{g}_1\|}, \vec{e}_2.\vec{e}_1 = 0, \|\vec{e}_2\| = 1 \qquad (62)$$

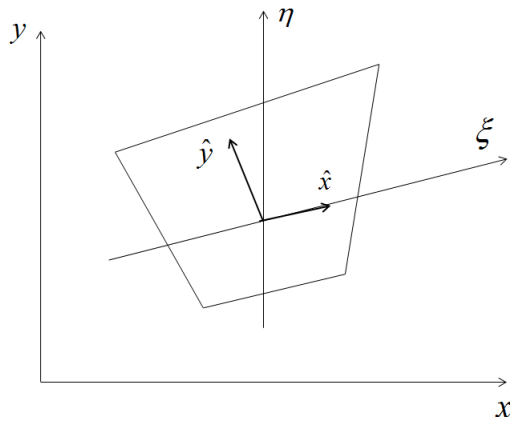

Figure 2: Corotational definition of the Q4 element.

All the operators in the form of a vector or matrix and the various mechanical fields (stress tensor, strain rate tensor, internal variable tensor) will be transported into the corotational coordinate frame in order to guarantee the objectivity of the tensorial increments. Only the nodal elementary forces (internal and external) will be turned at the end of the calculation in the global reference of the part. The gradient operator $[B^a_{n+1/2}]$ is decomposed into two parts: the strain tensor $[B^0_{n+1/2}]$ which gives the overall strain rate components $\{\dot{\varepsilon}^a\}_{n+1}$ in the center of the element ($\xi = \eta = 0$); and the tensor $[B^{ha}_{n+1/2}] = \xi[B^{\xi}_{n+1/2}] + \eta[B^{\eta}_{n+1/2}]$ that completes the formulation of the strain rate tensor components for any other point of the element and can be expressed as:

$$[B^0_{n+1/2}] = \begin{bmatrix} \langle b_x \rangle & \langle 0 \rangle \\ \langle 0 \rangle & \langle b_y \rangle \\ \langle b_y \rangle & \langle b_x \rangle \end{bmatrix} \qquad (63)$$

with $\{b_x\} = \frac{\partial \{N\}}{\partial x} \mid_{(\xi=\eta=0)}$, $\{b_y\} = \frac{\partial \{N\}}{\partial y} \mid_{(\xi=\eta=0)}$, and where (x, y) being the

coordinates of an arbitrary point in the corotational space frame.

Finally, the assumed strain rate field can be expressed under the following analytical form:

$$\left\{ \begin{array}{c} \Delta\varepsilon_x^0 \\ \Delta\varepsilon_y^0 \\ 2\Delta\varepsilon_{xy}^0 \end{array} \right\}_{(\xi=\eta=0)} = [B_{n+1/2}^0]\{\Delta U_{n+1}\} \tag{64}$$

with

$$\left\{ \begin{array}{l} \langle \Delta U_{n+1} \rangle = \langle \ \langle \Delta U_x \rangle \quad \langle \Delta U_y \rangle \ \rangle \\ \langle \Delta U_x \rangle = \ \langle \Delta u_{x1} \quad \Delta u_{x2} \quad \Delta u_{x3} \quad \Delta u_{x4} \rangle_{n+1} \\ \langle \Delta U_y \rangle = \langle \ \Delta u_{y1} \quad \Delta u_{y2} \quad \Delta u_{y3} \quad \Delta u_{y4} \rangle_{n+1} \end{array} \right. \tag{65}$$

The form of the second part of the gradient operator is based on the expression developed by Wang [30]. To eliminate volumetric and shear locking phenomena, an assumed strain rate field is proposed to replace the classical strain rate fields obtained by a symmetric gradient operator. Hence, the volumetric energy and the shear energy corresponding to the hourglass terms tend to be zero. So, we use the following assumed strain rate field:

$$\left\{ \begin{array}{l} \{\dot{\varepsilon}^a\}_{n+1} = \left\{ \begin{array}{c} \Delta\varepsilon_x^a \\ \Delta\varepsilon_y^a \\ 2\Delta\varepsilon_{xy}^a \end{array} \right\} = [B_{n+1/2}^a]\{\dot{u}^e\}_{n+1/2} \\ = [B_{n+1/2}^0]\{\dot{u}^e\}_{n+1/2} + (\xi[B_{n+1/2}^\xi] + \eta[B_{n+1/2}^\eta])\{\dot{u}^e\}_{n+1/2} \\ = \left\{ \begin{array}{c} \Delta\varepsilon_x^0 \\ \Delta\varepsilon_y^0 \\ 2\Delta\varepsilon_{xy}^0 \end{array} \right\} + \left\{ \begin{array}{c} \Delta\varepsilon_x^{ha} \\ \Delta\varepsilon_y^{ha} \\ 2\Delta\varepsilon_{xy}^{ha} \end{array} \right\} \end{array} \right. \tag{66}$$

with

$$\left\{ \begin{array}{l} \left[B_{n+1/2}^{ha}\right] = \xi \left[B_{n+1/2}^\xi\right] + \eta \left[B_{n+1/2}^\eta\right] \\ = \xi \left[\begin{array}{cc} \frac{1}{2}\langle b_{x\xi} \rangle & -\frac{1}{2}\langle b_{y\xi} \rangle \\ -\frac{1}{2}\langle b_{x\xi} \rangle & \frac{1}{2}\langle b_{y\xi} \rangle \\ \langle 0 \rangle & \langle 0 \rangle \end{array} \right] + \eta \left[\begin{array}{cc} \frac{1}{2}\langle b_{x\eta} \rangle & -\frac{1}{2}\langle b_{y\eta} \rangle \\ -\frac{1}{2}\langle b_{x\eta} \rangle & \frac{1}{2}\langle b_{y\eta} \rangle \\ \langle 0 \rangle & \langle 0 \rangle \end{array} \right] \end{array} \right. \tag{67}$$

where

$$\{b_{x\xi}\} = -\frac{1}{4J_{\xi\eta}}\left(\langle\xi\rangle\{Y\}\right)\{\boldsymbol{\gamma}\}, \{b_{x\eta}\} = \frac{1}{4J_{\xi\eta}}\left(\langle\eta\rangle\{Y\}\right)\{\boldsymbol{\gamma}\}$$
$$\{b_{y\xi}\} = \frac{1}{4J_{\xi\eta}}\left(\langle\xi\rangle\{X\}\right)\{\boldsymbol{\gamma}\}, \{b_{y\eta}\} = -\frac{1}{4J_{\xi\eta}}\left(\langle\eta\rangle\{X\}\right)\{\boldsymbol{\gamma}\} \tag{68}$$

with $\langle X\rangle = \langle\ x_1 \quad x_2 \quad x_3 \quad x_4\ \rangle$ and $\langle Y\rangle = \langle\ y_1 \quad y_2 \quad y_3 \quad y_4\ \rangle$ the coordinates of the node in the corotational coordinate frame and $J_{\xi\eta}$ the determinant of the element jacobian matrix. The vector $\{\boldsymbol{\gamma}\}$ is calculated by the following expression:

$$\{\boldsymbol{\gamma}\} = -\frac{1}{4}\left[\{h\} - (\langle h\rangle\{X\}\{b_x\} - (\langle h\rangle\{Y\}\{b_y\}\right] \tag{69}$$

It is called hourglass stabilization vector, identical to the $\{\boldsymbol{\gamma}\}$-projection operator proposed by Belytschko [51].

The assumed Cauchy stress tensor at the $n+1$ step is updated from calling the elastoplastic behavior model:

$$\left\{\begin{array}{l} \{\underline{\sigma}^a_{n+1}\}_{\xi,\eta} = \left\{\begin{array}{c}\sigma_x\\ \sigma_y\\ \sigma_{xy}\end{array}\right\} = \{\underline{\sigma}^a_n\}_{\xi,\eta} + [C^{ep}]_{\xi,\eta}\{\Delta\underline{\varepsilon}^a_{n+1}\}_{\xi,\eta} \\ = \{\underline{\sigma}^a_{n+1}\}_{0,0} + \xi\{\underline{\sigma}^{\xi}_{n+1}\}_{\xi,\eta} + \eta\{\underline{\sigma}^{\eta}_{n+1}\}_{\xi,\eta} \end{array}\right. \tag{70}$$

where $[C^{ep}]_{\xi,\eta}$ is the material tangent modulus matrix of the elastoplastic behavior model.

The vector of the nodal internal forces is then evaluated by mixed integration Gauss points as:

$$\{R^e_M\}_{n+1} = \{R^0_M\}_{n+1} + \{R^{ha}_M\}_{n+1} \tag{71}$$

with

$$\{R^0_M\}_{n+1} = \underbrace{\int_{\Omega_e}\left[B^0_{n+1/2}\right]^T\{\underline{\sigma}^a_{n+1}\}_{0,0}d\Omega}_{1GP}$$
$$= \int_{-1}^{+1}\int_{-1}^{+1}\left[B^0_{n+1/2}\right]^T\{\underline{\sigma}^a_{n+1}\}_{0,0}J_0 d\xi d\eta = \left[B^0_{n+1/2}\right]^T\{\underline{\sigma}^a_{n+1}\}_{0,0}A \tag{72}$$

where A is the area of the element.

$$\{R_M^{ha}\}_{n+1} = \underbrace{\int_{\Omega_e} \left(\xi \left[B^{\xi}_{n+1/2}\right]^T + \eta \left[B^{\eta}_{n+1/2}\right]^T\right) \{\underline{\sigma}^a_{n+1}\}_{\xi,\eta} d\Omega}_{4GP}$$
$$= \int_{-1}^{+1}\int_{-1}^{+1} \left(\xi \left[B^{\xi}_{n+1/2}\right]^T + \eta \left[B^{\eta}_{n+1/2}\right]^T\right) \{\underline{\sigma}^a_{n+1}\}_{\xi,\eta} J_{\xi,\eta} d\xi d\eta \tag{73}$$
$$= \sum_{I=1}^{4} \omega_I^G \left(\xi_I^G \left[B^{\xi}_{n+1/2}\right]^T + \eta_I^G \left[B^{\eta}_{n+1/2}\right]^T\right) \{\underline{\sigma}^a_{n+1}\}_{\xi_I^G,\eta_I^G} J_{\xi_I^G,\eta_I^G}$$

with:

$$\begin{aligned} \omega_1^G &= \omega_2^G = \omega_3^G = \omega_4^G = 1 \\ \xi_1^G &= -\frac{1}{\sqrt{3}}, \xi_2^G = \frac{1}{\sqrt{3}}, \xi_3^G = \frac{1}{\sqrt{3}}, \xi_4^G = -\frac{1}{\sqrt{3}} \\ \eta_1^G &= -\frac{1}{\sqrt{3}}, \eta_2^G = \frac{1}{\sqrt{3}}, \eta_3^G = \frac{1}{\sqrt{3}}, \eta_4^G = -\frac{1}{\sqrt{3}} \end{aligned} \tag{74}$$

In the same way the stiffness matrix is integrated with a mixed Gauss Legendre integration scheme:

$$[K^e_{MM}]_{n+1} = \left[K^0_{MM}\right]_{n+1} + \left[K^{ha}_{MM}\right]_{n+1} = \left[B^0_{n+1/2}\right]^T [C^{ep}]_{0,0} \left[B^0_{n+1/2}\right] A$$
$$+ \sum_{I=1}^{4} \omega_I^G \left[B^{ha}_{n+1/2}\right]^T_{\xi_I^G,\eta_I^G} [C^{ep}]_{\xi_I^G,\eta_I^G} \left[B^{ha}_{n+1/2}\right]_{\xi_I^{PG},\eta_I^G} J_{\xi_I^G,\eta_I^G} \tag{75}$$

Diffusional aspects of the numerical derivation. The standard formulation has been selected to build the diffusion part of the element. This allows us deriving the following form for an elementary volume:

$$\int_{\Omega_e} (\delta c_H^L)^T D^* \dot{c}_H^L d\Omega + \int_{\Omega_e} (\overrightarrow{\nabla} \delta c_H^L)^T D^{**} \overrightarrow{\nabla} c_H^L d\Omega$$
$$+ \int_{\Omega_e} (\delta c_H^L)^T \theta_H^T \frac{dN^T}{d\varepsilon^p} \frac{d\varepsilon^p}{dt} d\Omega + \int_{\Omega_e} \left(\overrightarrow{\nabla} \delta c_H^L)^T \{CPT\}\right) d\Omega \tag{76}$$

with D^{**} as defined in appendix and $CPT = D^{ep}\vec{\nabla}\varepsilon^{ep} + D^{da}\vec{\nabla}D + D^p\vec{\nabla}p$ (see appendix). We discretize this variational form in an elementary domain and we focus on an typical element Ω_e at the instants t_{n+1} by switching to matrix notations. The same interpolation functions N_i, as for mechanical part, are used to approximate the lattice concentration of the element (Eqs. 60 and 61).

With these shape functions, we have at the $n+1$ step, with c_H^{lN} the nodes lattice concentration:

$$\begin{aligned} c_H^L &= \langle N \rangle \left\{ c_H^{lN} \right\}, \vec{\nabla} c_H^L = [B_D] \left\{ c_H^{lN} \right\}, \dot{c}_H^L = \langle N \rangle \left\{ \dot{c}_H^{lN} \right\} \\ \delta c_H^L &= \langle N \rangle \left\{ \delta c_H^{lN} \right\}, \vec{\nabla} \delta c_H^L = [B_D] \left\{ \delta c_H^{lN} \right\} \end{aligned} \tag{77}$$

Contrary to mechanical element, no transposition is needed for the diffusion element. The gradient operator $[B_D]$ is given by:

$$[B_D] = \begin{bmatrix} \frac{\partial \langle N \rangle}{\partial x} \\ \frac{\partial \langle N \rangle}{\partial y} \end{bmatrix} \tag{78}$$

The residue vector and the tangent matrix of diffusion are then evaluated (from Eq. 76) at the same integration Gauss point (ξ_I^G, η_I^G), with the same weighting coefficients ω_I^G as for the mechanical element:

$$\begin{aligned} \{R_D^e\} = & \underbrace{\int_{\Omega_e} \left(\{N\} D^* \langle N \rangle \left\{ \frac{\Delta c_H^{LN}}{\Delta t} \right\} + [B_D]^T D^{**} [B_D] \left\{ c_H^{LN} \right\} \right) d\Omega}_{4GP} \\ & + \underbrace{\int_{\Omega_e} \left(\{N\} \theta_H^T \frac{dN^T}{d\varepsilon^p} \frac{d\varepsilon^p}{dt} + [B_D]^T \{CPT\} \right) d\Omega}_{4GP} \\ = & \int_{-1}^{+1} \int_{-1}^{+1} \left(\{N\} D^* \langle N \rangle \left\{ \frac{\Delta c_H^{LN}}{\Delta t} \right\} + [B_D]^T D^{**} [B_D] \left\{ c_H^{LN} \right\} \right) J_{\xi,\eta} d\xi d\eta \\ & + \int_{-1}^{+1} \int_{-1}^{+1} \left(\{N\} \theta_H^T \frac{dN^T}{d\varepsilon^p} \frac{d\varepsilon^p}{dt} + [B_D]^T \{CPT\} \right) J_{\xi,\eta} d\xi d\eta \\ = & \sum_{I=1}^{4} \omega_I^G \left(\{N\} D^* \langle N \rangle \left\{ \frac{\Delta c_H^{LN}}{\Delta t} \right\} + [B_D]^T D^{**} [B_D] \left\{ c_H^{LN} \right\} \right) J_{\xi_I^G, \eta_I^G} \\ & + \sum_{I=1}^{4} \omega_I^G \left(\{N\} \theta_H^T \frac{dN^T}{d\varepsilon^p} \frac{d\varepsilon^p}{dt} + [B_D]^T \{CPT\} \right) J_{\xi_I^G, \eta_I^G} \end{aligned} \tag{79}$$

$$[K^e_{DD}] = \underbrace{\int_{\Omega_e} \left(\{N\} \frac{D^*}{\Delta t} \langle N \rangle + \{N\} \frac{\partial D^*}{\partial c^L_H} \frac{\Delta c^L_H}{\Delta t} \langle N \rangle + [B_D]^T D^{**} [B_D] \right) d\Omega}_{4GP}$$
$$+ \underbrace{\int_{\Omega_e} \{N\} \theta^T_H \frac{\partial}{\partial c^L_H} \left(\frac{dN^T}{d\varepsilon^p} \frac{d\varepsilon^p}{dt} \right) \langle N \rangle + [B_D]^T \frac{\partial}{\partial c^L_H} \{CPT\} \langle N \rangle d\Omega}_{4GP}$$
$$= \sum_{I=1}^{4} \omega^G_I \left(\{N\} \frac{D^*}{\Delta t} \langle N \rangle + \{N\} \frac{\partial D^*}{\partial c^L_H} \frac{\Delta c^L_H}{\Delta t} \langle N \rangle + [B_D]^T D^{**} [B_D] \right) J_{\xi^G_I, \eta^G_I}$$
$$+ \sum_{I=1}^{4} \omega^G_I \left(\{N\} \theta^T_H \frac{\partial}{\partial c^L_H} \left(\frac{dN^T}{d\varepsilon^p} \frac{d\varepsilon^p}{dt} \right) \langle N \rangle + [B_D]^T \frac{\partial}{\partial c^L_H} \{CPT\} \langle N \rangle \right) J_{\xi^G_I, \eta^G_I} \quad (80)$$

3.3.3. Temporal stability for diffusion analysis

Time integration in transient diffusion analysis is done with the backward Euler method, which is unconditionally stable for linear problems. Time incrementation can be automatic or fixed, but automatic one is generally preferred because the response is usually simple diffusion: the rate of change of normalized concentration varies widely during the step and requires different time increments to maintain accuracy of the numerical scheme during the time integration. However, spurious oscillations can be observed due to small time increments.

To avoid these spurious oscillations or small time increments in transient mass diffusion analysis, the way is different depending on the order of the considered elements. For example with second-order elements, one can use the following relationship between the minimum usable time step and the element size:

$$\Delta t > \frac{\Delta l^2}{6D} \quad (81)$$

where Δt is the time increment, D is the diffusivity, and Δl is a typical element dimension (such as the length of a side of an element). If time increments smaller than this value are used, spurious oscillations can appear in the solution.

Therefore one must ensure that the given value does not violate the above criterion.

When transient analysis uses first-order elements, that is presently used, such oscillations are eliminated (the solubility terms are lumped), but can lead to locally inaccurate solutions for small time increments. In the case where smaller time increments are required, a finer mesh should be used in regions where the normalized concentration changes occur.

Generally there is no upper limit on the time increment because the integration procedure is unconditionally stable unless nonlinearities cause numerical problems. In the present work with nonlinearities, we make sure that the condition in Eq. 81 is satisfied for all the simulations.

3.3.4. Implemantation of the 2D multiphysic element in Abaqus/standard FEM software

To facilitate the writing of this element in the subroutine UEL, we decided to substitute the DOF initially used for the temperature (noted NT11 in Abaqus) by the DOF of concentration. The numerical scheme for the resolution of the thermomechanical equations is very close to the numerical scheme of the mechanical/diffusion proposed in this article. So, a classical "Coupled temp-displacement" solver option has been selected.

UEL objective is to compute the vector RHS and the matrix AMATRX, which correspond, for our coupled mechanical-diffusion element, respectively to the residue R (right hand of Eq. 46) and the element matrix $[K^e]$ (left hand of Eq. 46, without the increment vector). We give in Fig. 3 the flowchart of the implementation in Abaqus, with the UEL expansion in Fig. 4.

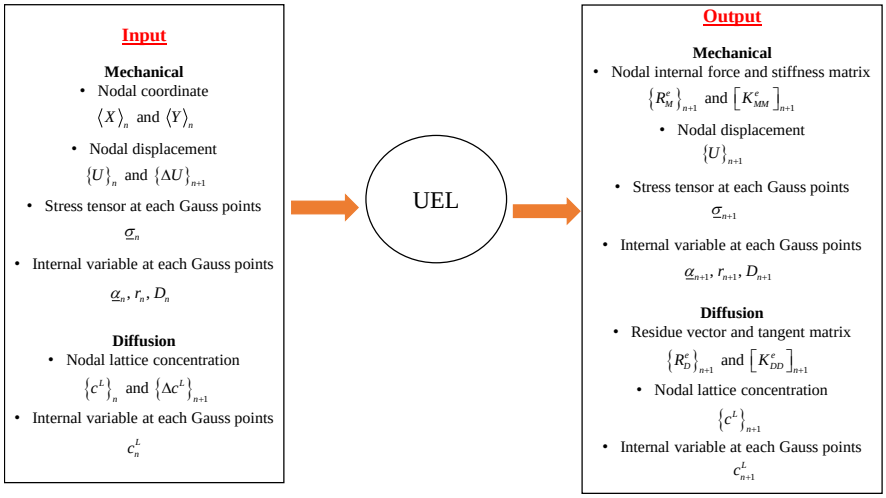

Figure 3: Implementation flowchart in Abaqus.

UEL

Mechanical	Diffusion
Computation of the rotation tensor at $t = t_n$ and $t = t_{n+1}$ $\langle X \rangle_n$ and $\langle Y \rangle_n \rightarrow [Q]_n$ $\langle X \rangle_{n+1}$ and $\langle Y \rangle_{n+1} \rightarrow [Q]_{n+1}$ Rotation in the corotational frame $[Q]_n$	
Gauss point loop • Computation of the operator $\langle N \rangle_n$, $[B^0_{n+1/2}]$, $[B^\xi_{n+1/2}]$, $[B^\eta_{n+1/2}]$ • Computation of the strain rate $\Delta\tilde{\underline{\varepsilon}}_{n+1}$ • Update of the stress tensor $\tilde{\underline{\sigma}}_{n+1} = \tilde{\underline{\sigma}}_n + [C^{ep}]\Delta\tilde{\underline{\varepsilon}}_{n+1}$ • Rotation of the stress tensor in the initial frame $\underline{\sigma}_{n+1} = [Q]^T_{n+1}\tilde{\underline{\sigma}}_{n+1}[Q]_{n+1}$ • Computation of the force vector and stiffness matrix $\{\tilde{R}^e_M\}_{n+1}$ and $[\tilde{K}^e_{MM}]_{n+1}$ • Rotation of the force vector and stiffness matrix $\{R^e_M\}_{n+1} = [Q]^T_{n+1}\{\tilde{R}^e_M\}_{n+1}[Q]_{n+1}$ $[K^e_{MM}]_{n+1} = [Q]^T_{n+1}[\tilde{K}^e_{MM}]_{n+1}[Q]_{n+1}$	**Gauss point loop** • Computation of the operator $[B_D]$ • Computation of the residue vector and tangent matrix $\{R^e_D\}$ and $[K^e_{DD}]$

Figure 4: Inside the UEL.

4. Application to hydrogen diffusion in a metallic welded joint over long times

4.1. Input data

The described model is applied to the hydrogen diffusion in a metallic welded joint (junction of two identical materials). The welded metal has three zones: the Fused Zone (FZ), which corresponds to the material passed from the solid state to the liquid state during the welding operation; the Heat Affected Zone (HAZ), which is the seat of metallurgical modifications taking place only in the solid state; and the Base Metal (BM), which designates the target material that has not undergone any significant modification during the welding operation.

The mechanical parameters for BM and FZ have been identified experimentally and HAZ parameters can be chosen as the average of the BM and FZ parameters [52]. Only Young modulus E and the initial yield strength σ_{Y0} are different in each zone. Table 1 presents these values. For all zones, elastoplastic behaviour model with mixed hardening (kinematic and isotropic) strongly coupled with ductile isotropic damage has been used, with: Poisson's ratio $\nu = 0.33$, isotropic hardening parameters $Q = 3800$ MPa and $b = 15$, kinematic hardening parameters $C = 69500$ MPa and $a = 240$, damage evolution parameters $S = 12$ MPa, $s = 1.2$, $\beta = 1$, $Y_0 = 0$ MPa, $\gamma = 4$ and $D_c = 0.99$.

Table 1: Elasto-plastic and diffusion parameters

Parameters	Base metal	Heat affected zone	Fused zone
E (MPa)	132000	124000	115000
σ_{Y_0} (MPa)	777	796	812
D_{H0}^{L} $(mm^2/year)$	4.005×10^5	4.505×10^5	5.005×10^5
D_{H0}^{T} $(mm^2/year)$	1.428×10^{-5}	1.482×10^{-5}	1.646×10^{-5}

For hydrogen diffusion parameters, due to the lack of experimental data, only diffusion coefficients are assumed to be different for the three zones (see Table 1). The BM parameters are from literature [5, 12, 13]. The others are chosen in

relation to our application. It has been assumed that there is greater diffusion in the FZ than in the BM. For all zones: a zero initial hydrogen concentration is prescribed ($c_{H0}^L = c_{H0}^T = 0$), $\beta = 6.67 \times 10^{-3}\ m^3/mol$, $\Delta\mu_H^b = 60\ kJ/mol$, $N^L = 8.47 \times 10^5\ mol/m^3$ and Eq. 39 is used for N^T modeling. No hydrogen flow was applied ($\bar{J}_H = 0$). Dirichlet boundary condition is applied with $c_H^{Le} = 3.46 \times 10^{-3} mol/m^3$ to the left of the material. Fig. 5 shows the schematic geometry used and boundary conditions. The Onsager kinetic coefficients of barodiffusion are taken equal to zero ($L_{Hp}^L = L_{Hp}^T = 0$) for all zones.

As mentioned previously, temperature is supposed to be constant with $T = 300K$. The total time of simulation is $t = 125$ years that corresponds to specific use of this material/structure (as for example storage). The maximum size of the elements is 1.91 mm. Therefore, with diffusivity of $4.005 \times 10^5 mm^2/\text{year}$, the minimum time increment to ensure time stability will be 1.51×10^{-6} year. In the simulations, we set a minimum of 10^{-5} year as temporal discretization increment. This allows us to ensure the condition given in Eq. 81.

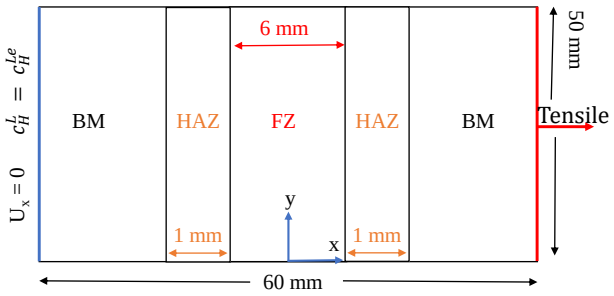

Figure 5: schematic geometry and boundary conditions.

4.2. General results

General results are presented in this subsection to show the distribution of hydrogen lattice concentration c_H^L/c_H^{Le} (Fig. 6), the distribution of trapped hydrogen concentration c_H^T/c_H^{Le} (Fig. 7), the distribution of equivalent plastic strain ε^p (Fig. 8) and the distribution of damage variable D (Fig. 9) at $t =$ 1 year, $t = 25$ years, $t = 75$ years and $t = 125$ years. At $t = 1$ year, no plasticity or damage is observed. At this time ($t = 1$ year), hydrogen lattice and

trapped concentration distributions follow the one of the hydrostatic pressure (see Eqs. 91 and 93 in appendix) and are linear. At $t = 25$ years, the trapped hydrogen concentration distribution becomes non-linear because of plasticity and/or damage. This is explained by the Eq. 40 of the trapped hydrogen concentration evolution, which is strongly linked to the plasticity (thus to the damage). At this time ($t = 25$ years), lattice hydrogen distribution remains almost linear. It is only after $t = 25$ years that we begin to observe the effects of plasticity and/or damage on the lattice hydrogen concentration distribution.

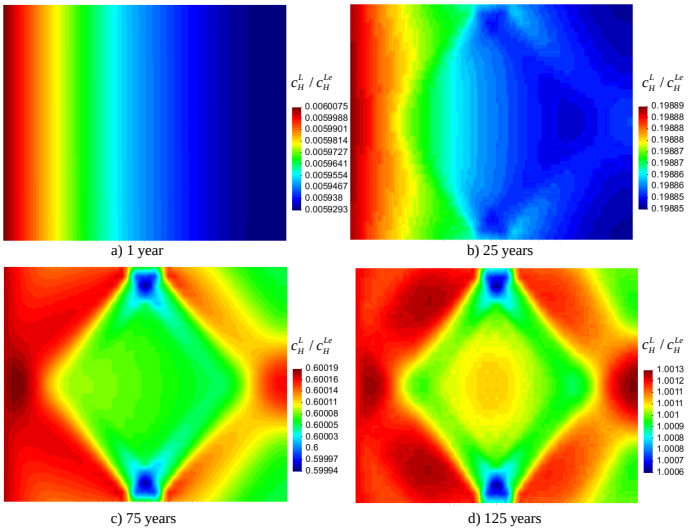

Figure 6: Normalized lattice c_H^L / c_H^{Le} concentration distribution with time.

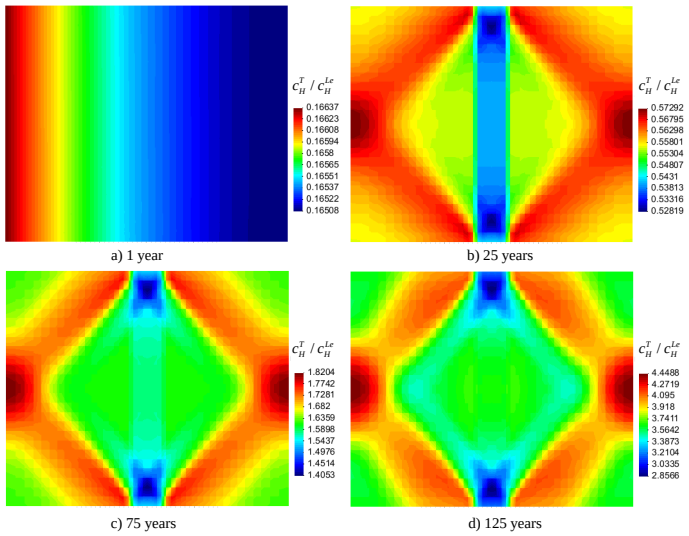

Figure 7: Normalized trapped c_H^T/c_H^{Le} concentration distribution with time.

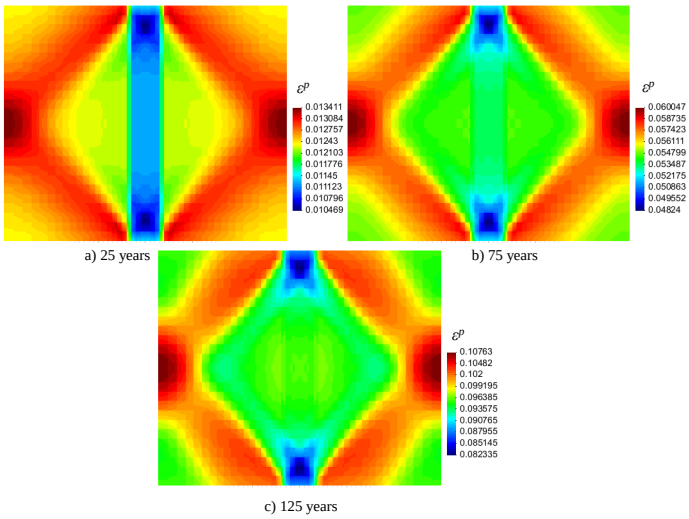

Figure 8: Equivalent plastic strain ε^p distribution with time.

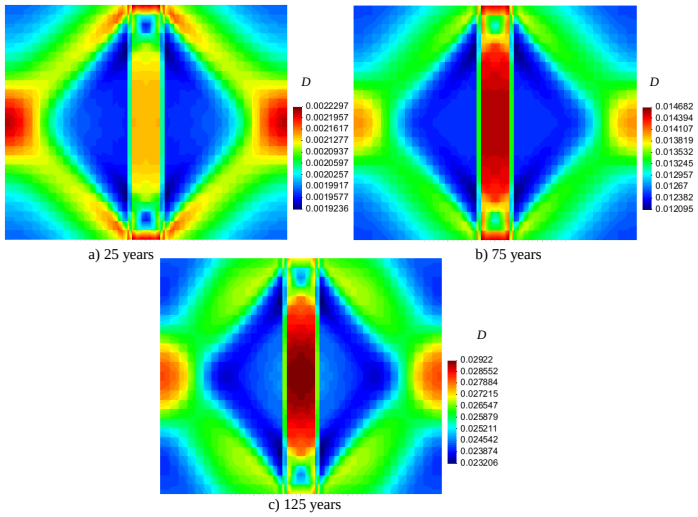

Figure 9: Damage variable D distribution with time.

With respect to c_H^L/c_H^{Le}, c_H^T/c_H^{Le}, D and ε^p variations, the maximum value of θ_H^L and θ_H^T is respectively 4.1×10^{-9} and 1.92×10^{-12}. This validates numerically the definition of Eq. 36 and the assumption that supposing $\theta_H^L \ll 1$ in Eq. 38

In the rest of the following subsections, a horizontal section is made in the middle of the material to report on the results from numerical analysis for hydrogen diffusion in the welded metal. These results focus on diffusion in trapping sites (subsection 4.3), diffusion effects on damage and equivalent plastic strain (subsection 4.4) and damage effects on diffusion variables (subsection 4.5).

For the effects of mechanics on diffusion, this is no longer to be demonstrated because of the gradient of the hydrostatic pressure, which influences the lattice concentration c_H^L. Lattice concentration gradient remains uniformly linear without mechanics (uncoupled) compared to the case with mechanics M-D (coupled) (see Fig. 10). In addition, without coupling with the mechanics, the trap concentration remains constant because only depending on the plasticity of the material.

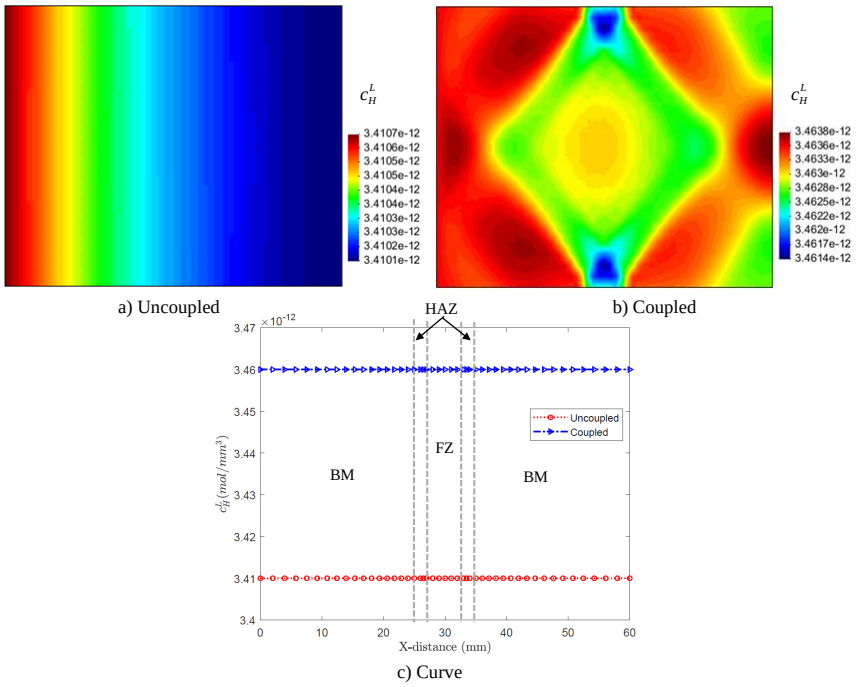

Figure 10: Lattice concentration distribution at $t = 125$ years: a) without mechanic coupling terms, b) with the actual M-D coupling, c) Comparison curve (middle of the horizontal section of the material).

4.3. Diffusion in trapping sites

Generally, mobility in trapping sites or equivalent diffusion coefficient is considered to be close to zero ($D_{H0}^T \approx 0$, see Table 1). This is because traps are not connected or because their deep potential energy well prevents hydrogen from diffusing. Consequently, flux in traps is usually assumed to be equal to zero: $\vec{J}_H^T = \vec{0}$ [5, 12]. Díaz [13] studied the effects of $\vec{J}_H^T$ at 130s and concluded that flux in trapping sites can be neglected.

In the present work, with a total time simulation of $t = 125$ years, we have to do a new study on the trapping diffusion effect on our results. We perform thus a simulation with D_H^T values as in Table 1 and a second simulation taking $D_{H0}^T = 0$ that implies $\vec{J}_H^T = \vec{0}$ for all zones. The softening parameter ξ is taken equal to 0.1, same value used by Sofronis [5]. Figure 11 shows the nor-

malized lattice hydrogen concentration c_H^L/c_H^{Le} (on the left) and the normalized trapping hydrogen concentration c_H^T/c_H^{Le} (on the right) with $\vec{J}_H^T$ and without $\vec{J}_H^T$. The comparison shows a very slight increase ($\approx 0.02\%$) in lattice hydrogen concentration with $\vec{J}_H^T \neq \vec{0}$ and practically no effect on trapping hydrogen concentration. No effect of $\vec{J}_H^T$ was also observed on equivalent plastic strain ε^p and damage variable D (see Fig. 12). It can be concluded from this study, as Daz [13], that flux in trapping sites can be neglected.

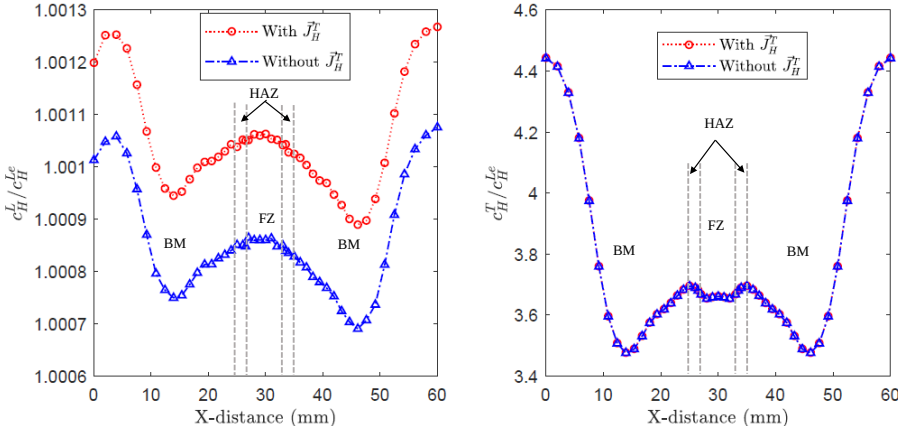

Figure 11: The normalized lattice c_H^L/c_H^{Le} (on the left) and trapping c_H^T/c_H^{Le} (on the right) hydrogen concentration with and without $\vec{J}_T$.

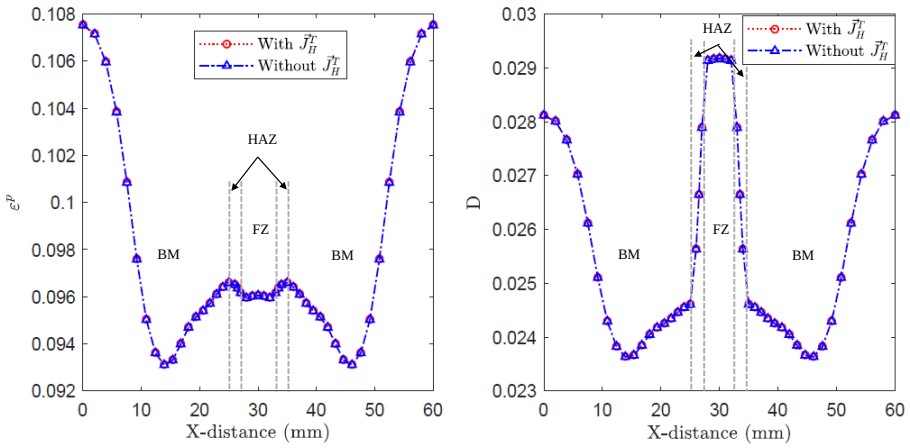

Figure 12: Equivalent plastic strain ε^p (on the left) and damage variable D (on the right) with and without $\vec{J}_T$.

4.4. Diffusion effects on damage and equivalent plastic strain evolution

The numerical results that we present here enable us to make a comparison between a pure mechanical model and the presently developed mechanical-diffusion (M-D) coupled model results. For this, two kinds of simulations are performed: one with only mechanical damage behaviour model and another with M-D model. Fig. 13 shows a distribution of equivalent plastic strain ε^p on the left and the damage variable D on the right, using both mechanical and M-D model, and corresponding to the end of simulation. The first remark is that whatever the model used (mechanical or M-D), the plasticity is higher in BM than in HAZ and FZ. This is mainly due to σ_{Y0} higher in the FZ and HAZ than in the BM (see Table 1). The second remark is that, with M-D model, the diffusion tends to increase the equivalent plastic strain. It agrees well with the existing conclusions in the literature: hydrogen softens metal [1] or metal and alloys are degraded in the presence of hydrogen [1, 2, 3, 4, 5].

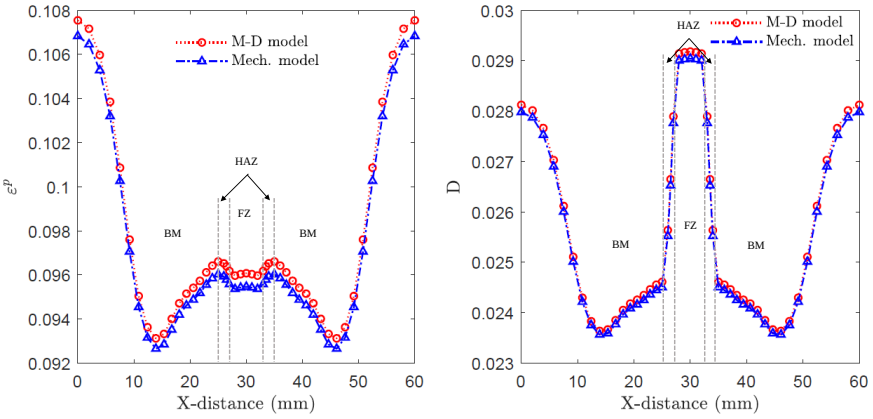

Figure 13: Equivalent plastic strain ε^p (to the left) and damage variable D (to the right): comparison between the mechanical model and the M-D model.

For damage variable distribution, an increasing trend with the M-D model is observed but has a very weak effect. This may be due to the fact that the material is not very plasticized and therefore less damaged (low Lagrange plastic multiplier). So, assuming that it is the hydrogen in the trapping sites that causes the most fragility of the material, the diffusion tends to have no significant influence on the damage. Contrarily to equivalent plastic strain, damage variable D increases more in FZ and HAZ than in BM. The explications for this fact can be seen on the evolution of damage conjugate force (Fig. 14) due to Eq. 28.

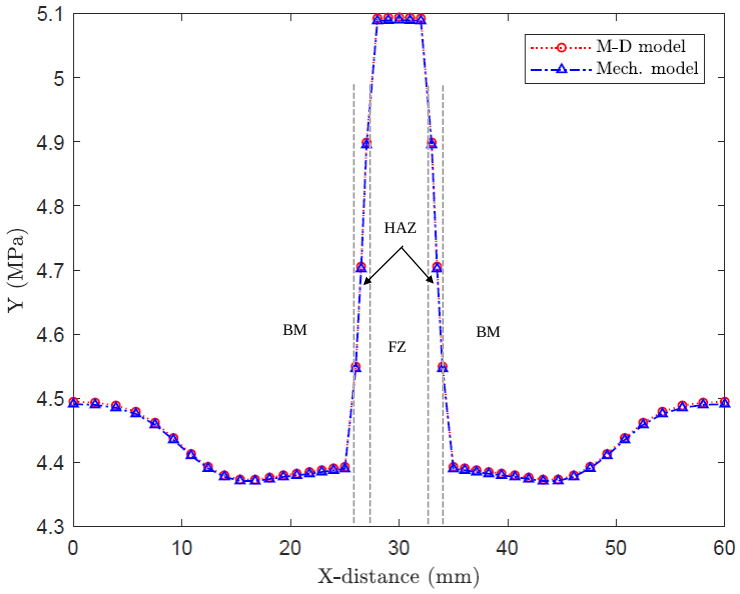

Figure 14: Damage conjugate force Y: comparison between the mechanical model and the M-D model.

Hydrogen softens and degrades metal and alloys. According to this result (and the evolution of equivalent plastic strain and damage obtained here), it is very important to take into account this phenomenon in the case of studying lifetime of a material in contact with severe environments.

4.5. Damage effects on diffusion variables

Our coupled theory for hydrogen diffusion takes into account damage and both kinematic and isotropic hardening. In this part, we specifically evaluate the influence of the damage on the evolution of hydrogen diffusion variables. Two simulations are made with M-D model: a simulation in which one deactivates the damage phenomenon, and a simulation in which one takes it into account. In Fig. 15, the normalized lattice c_H^L/c_H^{Le} (on the left) and trapping c_H^T/c_H^{Le} (on the right) hydrogen concentrations are presented. An increase is observed in the normalized lattice hydrogen concentration taking into account the damage phenomenon (an increase of more than 0.1% in BM). This evolution even tends to follow that of the equivalent plastic strain. Therefore, the gradient term of D

can not be ignored in the lattice hydrogen evolution equation (see Eq. 41 and Eqs. 91 to 94 in appendix).

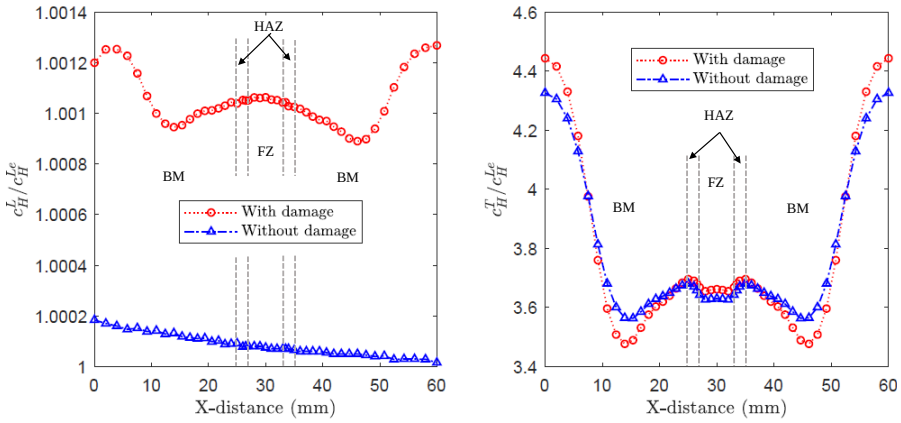

Figure 15: Damage effects on the normalized lattice c_H^L/c_H^{Le} (on the left) and trapping c_H^T/c_H^{Le} (on the right) hydrogen concentration.

For the trapping hydrogen concentration c_H^T, it is function of plasticity and therefore of the damage variable (see Eq. 38) due to the dependence of the number of moles of trapping sites to plasticity (Eq. 39). It should be noted that the cumulative plastic strain rate in the case where the damage phenomenon is taken into account is defined by $\dot{\varepsilon}^p = \dot{\delta}/\sqrt{1-D}$. Increase in trapping hydrogen concentration with damage is noted particularly in BM (between 0 and 8 mm and between 52 to 60 mm). A decrease is also observed in BM (between 10 and 20 mm and between 40 to 50 mm). The explanation is related to N^T and ε^p variation. Fig. 16 shows the number of moles of trapping sites N^T (on the left) and the equivalent plastic strain ε^p (on the right) evolution with and without damage. Damage in some case (increase in ε^p, thus in c_H^T) can be seen as traps for hydrogen.

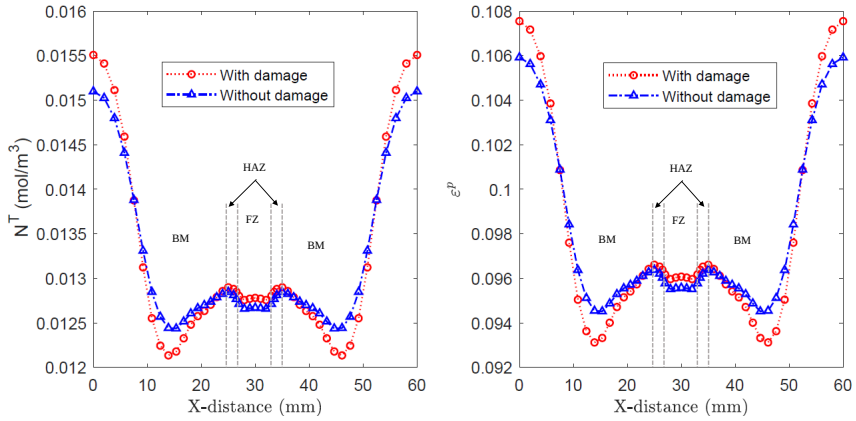

Figure 16: Damage effects on the number of moles of trapping sites N^T (on the left) and equivalent plastic strain ε^p (on the right).

5. Conclusion

A fully coupled thermo-elastoplastic and diffusion model has been presented from a theoretical point of view. This model includes both isotropic and kinematic hardening in the material, damage, and is based on the thermodynamics of irreversible processes with state variables and assuming the small deformation hypothesis. The different hydrogen concentrations are then introduced as internal variables, which allows obtaining chemical potentials as a derivative of state potential, taken equal to the Helmholtz specific free energy.

Numerical development of a multiphysic quadrilateral 2D element coupling mechanical to diffusion is proposed. This element uses an "assumed strain" formulation to build the mechanical part of the element to avoid the occurrence of volumetric expansion locking and shear locking; and the standard formulation to build the diffusion part. The 2D multiphysic element is then implemented in Abaqus/standard FEM software using the subroutine UEL. The numerical scheme for the resolution of the thermomechanical equations being very close to the numerical scheme of the mechanical/diffusion proposed in this article, a classical "Coupled temp-displacement" solver option has been selected then adapted to our resolution.

The coupled model leads to an increase in equivalent plastic strain and damage variable evolution due to diffusion. The study of diffusion in trapping sites leads to the conclusion that flux in trapping sites can be neglected. The evolution of equivalent plastic strain and damage variable obtained with the coupled model clearly enhances the effects of diffusion with mechanical behaviour. Therefore, it seems very important to take into account diffusion phenomenon in the case of lifetime studying of a material in contact with the environment, especially for prediction at long times. Damage effects on diffusion parameters cannot be neglected.

From an experimental point of view, it is possible to have partial validations of the present modelling, for examples for hydrogen with laboratory equipment [53]. However, one has first to remain that such experiments should be followed during a long time to be consistent with the proposed modelling. Actually, the experiments on mechanochemistry are performed during short times, less than a couple of years. Second, if temperature can be quite easily in-situ monitored, it is more difficult to have in-situ measurements for all the components of the strain or stress tensor or for damage effects, as well as to obtain accurate concentration of small molecules with high mobility such as hydrogen. These aspects remain yet to be investigated.

In future prospects, the effects of diffusion on mechanical properties such as Youngs modulus, Poissons ratio, and also on the evolution of damage variable will be proposed, by considering a direct coupling between damage and diffusion variables (chemical potentials, concentrations) as for mechanical variables.

Appendix

In this appendix, we develop the diffusion equations, especially the lattice hydrogen concentration evolution equation at constant temperature. Chemical potentials and fluxes expressions of lattice and trapping sites are given by Eqs. 82 to 85.

$$\mu_H^L = \mu_{H0}^L + R_g T \ln\left(\frac{\theta_H^L}{1-\theta_H^L}\right) - 3K\beta\sqrt{1-D}tr(\underline{\varepsilon}^e) \tag{82}$$

$$\mu_H^T = \mu_{H0}^T + R_g T \ln\left(\frac{\theta_H^T}{1-\theta_H^T}\right) - 3K\beta\sqrt{1-D}tr(\underline{\varepsilon}^e) \tag{83}$$

775

$$\vec{J}_H^L = -L_H^L\vec{\nabla}\mu_H^L - L_{Hp}^L\vec{\nabla}p \tag{84}$$

$$\vec{J}_H^T = -L_H^T\vec{\nabla}\mu_H^T - L_{Hp}^T\vec{\nabla}p \tag{85}$$

The gradient of lattice and trapping chemical potentials are calculated and given respectively by Eq. 86 and Eq. 87.

$$\vec{\nabla}\mu_H^L = \begin{cases} \dfrac{R_g T N^L}{(N^L - c_H^L)c_H^L}\vec{\nabla}c_H^L - 3K\beta\sqrt{1-D}\vec{\nabla}tr(\underline{\varepsilon}^e) \\ +\dfrac{3K\beta\sqrt{1-D}tr(\underline{\varepsilon}^e)}{2\sqrt{1-D}}\vec{\nabla}D \end{cases} \tag{86}$$

$$\vec{\nabla}\mu_H^T = \begin{cases} \dfrac{R_g T N^T}{(N^T - c_H^T)c_H^T}\left(\vec{\nabla}c_H^T - \dfrac{c_H^T\vec{\nabla}N^T}{N^T}\right) \\ -3K\beta\sqrt{1-D}\vec{\nabla}tr(\underline{\varepsilon}^e) + \dfrac{3K\beta\sqrt{1-D}tr(\underline{\varepsilon}^e)}{2\sqrt{1-D}}\vec{\nabla}D \end{cases} \tag{87}$$

We use Eq. 88 of Cauchy stress tensor to compute the gradient of the trace of elastic strain tensor given in Eq.89.

$$\underline{\sigma} = (1-D)\left(\lambda(\underline{\varepsilon}^e : \underline{1}) + 2\mu\underline{\varepsilon}^e\right) - 3K\sqrt{1-D}\left(\beta(\Delta c_H^L + \Delta c_H^T)\right)\underline{1} \tag{88}$$

$$3K\vec{\nabla}tr(\underline{\varepsilon}^e) = \begin{cases} \dfrac{\vec{\nabla}tr(\underline{\sigma})}{1-D} + 9K\beta\dfrac{\vec{\nabla}c_H^L + \vec{\nabla}c_H^T}{\sqrt{1-D}} \\ -\left(\dfrac{-tr(\underline{\sigma})}{(1-D)^2} - \dfrac{9K\beta}{2(1-D)^{3/2}}(\Delta c_H^L + \Delta c_H^T)\right)\vec{\nabla}D \end{cases} \tag{89}$$

The gradient of trapping hydrogen concentration is then calculated:

$$\begin{cases} c_H^T = \dfrac{N^T c_H^L K^T}{c_H^L K^T + N^L} \\ \vec{\nabla}c_H^T = \dfrac{c_H^T(1-\theta_H^T)}{c_H^L}\vec{\nabla}c_H^L + \theta_H^T\vec{\nabla}N^T \end{cases} \tag{90}$$

With $tr(\underline{\sigma}) = -3p$, the expressions of fluxes are in the following forms:

$$\begin{aligned} \vec{J}_H^L &= -D_L^{**}\vec{\nabla}c_H^L - D_L^{ep}\vec{\nabla}\varepsilon^{ep} - D_L^{da}\vec{\nabla}D - D_L^p\vec{\nabla}p \\ \vec{J}_H^T &= -D_T^{**}\vec{\nabla}c_H^L - D_T^{ep}\vec{\nabla}\varepsilon^{ep} - D_T^{da}\vec{\nabla}D - D_T^p\vec{\nabla}p \\ \vec{J}_H^L + \vec{J}_H^T &= -D^{**}\vec{\nabla}c_H^L - D^{ep}\vec{\nabla}\varepsilon^{ep} - D^{da}\vec{\nabla}D - D^p\vec{\nabla}p \end{aligned} \tag{91}$$

where:

$$\begin{cases} D_L^{**} = D_H^L - 9L_H^L K\beta^2 D^* \\ D_T^{**} = D_H^T(D^* - 1) - 9L_H^T K\beta^2 D^* \\ D_L^{ep} = -9L_H^L K\beta^2 \theta_H^T \dfrac{\partial N^T}{\partial \varepsilon^p} \\ D_T^{ep} = -9L_H^T K\beta^2 \theta_H^T \dfrac{\partial N^T}{\partial \varepsilon^p} \\ D_L^{da} = 3L_H^L \beta \left(\dfrac{p}{(1-D)^{3/2}} - \dfrac{3K\beta}{2(1-D)}(\Delta c_H^L + \Delta c_H^T) + \dfrac{Ktr(\underline{\varepsilon}^e)}{2\sqrt{1-D}} \right) \\ D_T^{da} = 3L_H^T \beta \left(\dfrac{p}{(1-D)^{3/2}} - \dfrac{3K\beta}{2(1-D)}(\Delta c_H^L + \Delta c_H^T) + \dfrac{Ktr(\underline{\varepsilon}^e)}{2\sqrt{1-D}} \right) \\ D_L^p = \dfrac{3L_H^L \beta}{\sqrt{1-D}} + L_{Hp}^L \\ D_T^p = \dfrac{3L_H^T \beta}{\sqrt{1-D}} + L_{Hp}^T \\ D^* = \dfrac{c_H^T(1-\theta_H^T) + c_H^L}{c_H^L} \\ D_H^L = \dfrac{L_H^L R_g T N^L}{(N^L - c_H^L)c_H^L} \\ D_H^T = \dfrac{L_H^T R_g T N^T}{(N^T - c_H^T)c_H^T} \\ D^{**} = D_L^{**} + D_T^{**} \\ D^{ep} = D_L^{ep} + D_T^{ep} \\ D^{da} = D_L^{da} + D_T^{da} \\ D^p = D_L^p + D_T^p \end{cases} \tag{92}$$

The lattice hydrogen concentration evolution equation at constant temperature can then be computed using Eq. 91:

$$D^* \dot{c}_H^L + \theta_H^T \frac{dN^T}{d\varepsilon^p} \frac{d\varepsilon^p}{dt} + \vec{\nabla} \cdot \vec{J}_H^L + \vec{\nabla} \cdot \vec{J}_H^T = 0 \tag{93}$$

The functional related to diffusion at constant temperature is given by Eq.94:

$$\{R_D\} = \begin{cases} \displaystyle\int_V \{N\} D^* \langle N \rangle dV \{\dot{c}_H^L\} + \int_V \{N\} \theta_H^T \left\{ \frac{dN^T}{d\varepsilon^p} \frac{d\varepsilon^p}{dt} \right\} dV \\ \displaystyle -\int_V [B_D]^T \{-D^{**} \vec{\nabla} c_H^L - D^{ep} \vec{\nabla} \varepsilon^{ep} - D^{da} \vec{\nabla} D - D^p \vec{\nabla} p\} dV \end{cases} \tag{94}$$

Acknowledgment

This work has been carried out by grants from the Grand Est region and the FEDER. The authors express their gratitude to this region and Europe.

References

[1] J. Hirth, Effects of hydrogen on the properties of iron and steel, Metallurgical Transactions A. 11 (1980) 861–890.

[2] I. M. Bernstein, The role of hydrogen in the embrittlement of iron and steel, Materials Science and Engineering 6 (1970) 1–19.

[3] R. A. Oriani, Hydrogen embrittlement of steels, Annual Review of Materials Science 8 (1978) 327–357.

[4] D. Delafosse, T. Magnin, Hydrogen induced plasticity in stress corrosion cracking of engineering systems, Engineering Fracture Mechanics 68 (2001) 693–729.

[5] P. Sofronis, Y. Liang, N. Aravas, Hydrogen induced shear localization of the plastic flow in metals and alloys, European Journal of Mechanics A/Solids 20 (2001) 857–872.

[6] R. A. Oriani, P. H. Josephic, Equilibrium aspects of hydrogen-induced cracking of steels, Acta Metallurgica 22 (1974) 1065–1074.

[7] W. W. Gerberich, Y. T. Chen, Hydrogen-controlled cracking - an approach to threshold stress intensity, Metallurgical Transactions A 6 (1975) 271–278.

[8] H. K. Birnbaum, P. Sofronis, Hydrogen-enhanced localized plasticity - a mechanism for hydrogen-related fracture, Materials Science and Engineering: A 176 (1994) 191–202.

[9] J. Lufrano, P. Sofronis, H. K. Birnbaum, Modeling of hydrogen transport and elastically accommodated hydride formation near a crack tip, Journal of the Mechanics and Physics of Solids 44 (1996) 179–205.

[10] J. Lufrano, P. Sofronis, H. K. Birnbaum, Elastoplastically accommodated hydride formation and embrittlement, Journal of the Mechanics and Physics of Solids 46 (1998) 1497–1520.

[11] A. Taha, P. Sofronis, A micromechanics approach to the study of hydrogen transport and embrittlement, Engineering Fracture Mechanics 68 (2001) 803–837.

[12] C. V. Di Leo, L. Anand, Hydrogen in metals: a coupled theory for species diffusion and large elasticplastic deformations, International Journal of Plasticity 43 (2013) 42–69.

[13] A. Daz, J. M. Alegre, I. I. Cuesta, Coupled hydrogen diffusion simulation using a heat transfer analogy, International Journal of Mechanical Sciences 115–116 (2016) 360–369.

[14] R. A. Oriani, The diffusion and trapping of hydrogen in steel, Acta Metallurgica 18 (1970) 147–157.

[15] J. Lemaitre, J. L. Chaboche, Mécanique des matériaux solides, Dunod, Paris (1985).

[16] J. Lemaitre, A course of damage mechanics, Berlin, Springer Verlag (1992).

[17] J. Lemaitre, R. Desmorat, Engineering damage mechanics: Ductile, creep, fatigue, and brittle failures, Berlin, Springer (2005).

[18] K. Saanouni, Numerical modelling in damage mechanics, UK, Kogan Page Science (2003).

[19] F. A. McClintock, A criterion for ductile fracture by the growth of holes, Journal of Applied Mechanics 35 (1968) 363–371.

[20] J. R. Rice, D. M. Tracey, On the ductile enlargment of voids in triaxial stress fields, Journal of the Mechanics and Physics of Solids 17 (3) (1969) 201–217.

[21] A. Gurson, Continuum theory of ductile rupture by void nucleation and growth : Part 1 - yield criteria and flow rules for porous ductile media, Journal of Engineering Materials and Technology 99(2) (1977) 2–15.

[22] V. Tvergaard, Ductile fracture by cavity nucleation between larger voids, Journal of the Mechanics and Physics of Solids 30 (1982) 265–286.

[23] V. Tvergaard, Material failure by void growth to coalescence, Advances in Applied Mechanics 27 (1990) 83–151.

[24] J. L. Chaboche, Continuum damage mechanics: Part i- general aspects, Journal of Applied Mechanics 55 (1988) 59–64.

[25] J. L. Chaboche, Continuum damage mechanics: Part ii-damage growth, crack initiation and crack propagation, Journal of Applied Mechanics 55 (1988) 65–72.

[26] K. Saanouni, C. Forster, F. Benhatira, On the anelastic flow with damage, Int. J. of Damage Mechanics 3 (1994) 141–169.

[27] K. Saanouni, J. L. Chaboche, Computational damage mechanics. application to metal forming. chapter 7 of the volume 3: Numerical and computational methods (editors: R. de borst, h. a. mang), in comprehencive structural integrity, Edited by I. Milne, R.O. Ritchie and B. Karihaloo, ISBN: 0-08-043749-4 (2003).

[28] K. Saanouni, P. Lestriez, C. Labergere, 2D adaptive FE simulations in finite thermo-elasto-viscoplasticity with ductile damage: Application to orthogonal metal cutting by chip formation and breaking, Int. J. of Damage Mechanics 20 (2011) 23–61.

[29] K. Saanouni, Damage mechanics in metal forming: Advanced modeling and numerical simulation, Wiley (2012).

[30] J. Wang, J. Chen, M. Li, A uri 4-node quadrilateral element by assumed strain method for nonlinear problems, ACTA MECHANICA SINICA 20 (6) (2004) 632–641.

[31] K. Saliya, B. Panicaud, C. Labergere, Thermodynamics and multi-physical model for application to the effect of severe environment on metallic alloys, Technische MechaniK 38 (2018) 113–125.

[32] F. Fer, Thermodynamique macroscopique. 2, Cours et Documents de Chimie Series, Gordon & Breach Publishing Group, 1971.
URL https://books.google.fr/books?id=N8rQAAAAMAAJ

[33] C. Vidal, G. Dewel, P. Borckmans, Au-delà de léquilibre, Collection Enseignement Des Sciences, Hermann, 1994.

[34] P. Germain, Cours de mécaniques des milieux continus, Masson, Tome I, Paris (1973).

[35] J. P. Boehler, Lois de comportement anisotrope des milieux continus, Journal de Mécanique 17 (1978) N° 2.

[36] K. Saanouni, M. Hamed, H. Badreddine, C. Labergre, Ductile damage in metal forming: Advanced macroscopic modeling and numerical simulation. Chapter of the volume Damage Mechanics in Metal Forming in G. Voyiadjis (Editor) Handbook of Damage Mechanics: Nano to Macro Scale for Materials and Structures, Vol. 2, Springer, New York, 2015.

[37] B. Panicaud, L. Le Joncour, N. Hfaeidh, K. Saanouni, Micromechanical polycrystalline damage-plasticity modeling for metal forming processes. Chapter of the volume Damage Mechanics in Metal Forming in G. Voyiadjis (Editor) Handbook of Damage Mechanics: Nano to Macro Scale for Materials and Structures, Vol. 2, Springer, New York, 2015.

[38] J. Philibert, Atom movements: Diffusion and mass transport in solids, EDP Sciences. Les Ulis, France (1995).

[39] P. Sofronis, R. M. McMeeking, Numerical analysis of hydrogen transport near a blunting crack tip, Journal of the Mechanics and Physics of Solids 37 (1989) 317–350.

[40] A. H. M. Krom, R. W. J. Koers, A. D. Bakker, Hydrogen transport near a blunting crack tip, Journal of the Mechanics and Physics of Solids 47 (1999) 971–992.

[41] P. Lestriez, Modélisation numérique du couplage thermo-mécanique- endommagement en transformations finies : application à la mise en forme, PhD thesis, Université de Technologie de Troyes (2003).

[42] F. Sidoroff, A. Dogui, Some issues about anisotropic elastic-plastic models at finite strain, Int. J. of Solids and Structures 38 (2001) 9569–9578.

[43] H. Badreddine, Elastoplasticité anisotrope endommageable en grandes déformations: aspects théoriques, numériques et applications, PhD thesis, Université de Technologie de Troyes (2006).

[44] E. H. Lee, R. L. Mallet, T. B. Werhteimer, Stress analysis for anisotropic hardening in finite-deformation plasticity, J. Applied Mechanics 50 (1983) 554–560.

[45] F. Sidoroff, The geometrical concept of intermediate configuration and elastic plastic finite strain, Archives of Mechanics 25 (1973) 299–308.

[46] F. Sidoroff, Incremental constitutive equation for large strain elastoplasticity, Int. J. Engineering Science 20 (1982) 19–26.

[47] H. Badreddine, K. Saanouni, A. Dogui, On non-associative anisotropic finite plasticity fully coupled with isotropic ductile damage for metal forming, Int. J. of Plasticity 26 (2010) 1541–1576.

[48] T. J. R. Hughes, J. Winget, Finite rotation effects in numerical integration of rate- constitutive equations arising in large-deformation analysis, Int. J. for Numerical Methods in Engineering 15 (1980) 1862–1867.

[49] J. Fish, T. Belytschko, Elements with embedded localization zones for large deformation problems, Computers & Structures 30 (1-2) (1988) 247–256.

[50] J. Simo, T. Hughes, Computational inelasticity, Springer Verlag, New York (1998).

[51] T. Belytschko, W. K. Liu, B. Moran, Nonlinear finite elements for continua and structures, John Wiley, New York (2000).

[52] B. Sarre, Influence du soudage laser Nd:Yag sur les propriétés métallurgiques et mécaniques de l'alliage de titane TA6V, PhD thesis, Université de Technologie de Troyes (2018).

[53] A. Oudriss, F. Martin, X. Feaugas, Experimental techniques for dosage and detection of hydrogen, Mechanics - Microstructure - Corrosion Coupling (2019) 245–268.